2018

Modelling spatial heterogeneity in the haemodynamic response with implications for neuroimaging

Russell Gore
The University of Notre Dame Australia

Modelling spatial heterogeneity in the haemodynamic response with implications for neuroimaging

Russell Gore

This thesis is submitted for the degree of

Master of Science (Medicine)

School of Medicine

The University of Notre Dame, Australia

2018

I would like to dedicate this thesis to my loving and supportive wife, Natalie Gore, and my supervisors, Dr Edward Waters and Ben Hui.

...

Declaration

I hereby declare that except where specific reference is made to the work of others, the contents of this dissertation are original and have not been submitted in whole or in part for consideration for any other degree or qualification in this, or any other university. This dissertation is my own work and contains nothing which is the outcome of work done in collaboration with others, except as specified in the text and acknowledgements. This dissertation contains fewer than 65,000 words including appendices, bibliography, footnotes, tables and equations and has fewer than 150 figures.

Russell Gore

School of Medicine

The University of Notre Dame, Australia

2018

Acknowledgements

The time spent working on this thesis has been the most challenging and exciting time of my life. Along the way there were considerable changes that took place. Major changes occurred to the nature of my research project and within the first year of my degree I transferred schools. Sadly, I also experienced the loss of a great mentor and friend, my original supervisor, Dr Frank Moisiadis, in 2016. Regardless of these events, I am so glad I decided to pursue the ideas and issues found within these pages.

I would like to thank my original supervisors from Notre Dame University. Dr Frank Moisiadis, from the school of arts and sciences, encouraged me to overcome my fears and pursue mathematics and was the reason I chose to pursue a masters degree. Robert Anderson, my previous co supervisor, has been a great friend and mentor throughout my time as a student. I am so grateful to have met him and could not imagine being where I am today without all his help and encouragement.

I thank my current supervisors Dr Edward K. Waters, and Dr Ben Hui. Thank you Ben, for being so helpful in reviewing drafts and assessing the ideas and direction of my work. Edward has the remarkable ability of transforming an ordinary student into a focused and disciplined researcher with an eye for detail. He was always willing to donate his time, 24/7, to assist in developing the skills necessary to fast track my progress and develop a piece of research I can feel proud of. Thank you Edward for all your patience and the time you were willing to devote to my development as a research student moving into a new subject.

I thank the School of Medicine, Sydney, at The University of Notre Dame Australia, allowing the transfer of my candidature there to focus more on the biological interests in neuroimaging.

Finally, I thank all my friends, who were willing to support me through so many periods of absence while my head was stuck in the books. I am grateful to my parents, Margaret and Kelvin Gore, for supporting me through all the years of studying that lead up to this work. I am so lucky to have such supportive people in my life.

And finally, I thank my wife for supporting me through this time. I could not have done it without her support and encouragement.

Abstract

Background: A foundational assumption of neuroimaging is the central volume principle (CVP): the mean transit time of oxygen particles in the brain equals the ratio of blood vessel volume to blood flow. Changes in mean transit time are expected to cause detectable changes in images produced by functional magnetic resonance imaging (fMRI). The CVP assumes a uniform distribution of transit times, but in fact blood vessel volumes are spatially heterogeneous. This thesis examines the implications of spatial heterogeneity for fMRI research.

Methods: An amended form of the CVP that accounts for spatial heterogeneity is developed and parameterised using empirical data. Implications of spatial heterogeneity and oxygen extraction for fMRI research are then examined using computer simulations.

Results: Spatial heterogeneity significantly reduces mean transit times; however, parameterisation of the model shows that, contrary to expectation, transit times might be uniformly distributed rather than heterogeneous. Nonetheless, computer simulations showed that common experimental designs are inadequate to detect clinically meaningful changes in transit time. Again, contrary to expectation, oxygen extraction is found to have no significant effect on mean transit time.

Conclusion: This thesis casts doubt on the degree to which spatial heterogeneity causes problems in neuroimaging, but nonetheless reaffirms that existing experimental designs are

inadequate to detect significant changes in transit time. Further research on the assumption that significant changes in neuroimages are linked to changes in transit time is required.

Table of contents

List of figures

List of tables

Chapter 1

Introduction

1.1 About this thesis

The work in this thesis builds on the previous work by the supervisor and others [1], which use ordinary differential equations (ODEs, rather than partial differential equations) to model spatially heterogeneous population processes. In their paper, the authors used a linear functional relationship describing the relationship between the expected, or mean, value of a population variable and the associated variance to account for spatial heterogeneity. Taken together, the relationship between mean and variance is called mean crowding.[2, 3] The work in this thesis extends upon this prior work, and applies it in a new context: the haemodynamic response function (HRF) of the brain to neural stimuli.

1.2 Thesis outline

The outline of the thesis is as follows:

- Chapter 2 briefly reviews models of oxygen transport in the brain, and discusses the effect that the spatially and temporally heterogeneous nature of this phenomenon

has on interpreting the results of clinical research and diagnostics utilising modern neuroimaging technology, with particular focus on functional magnetic resonance imaging (fMRI).

- Chapter 3 considers the problem of the movement of a given particle of oxygen, typically described in fMRI research using the central volume principle (CVP), which relates the volume of a blood vessel to the transit time of a particle. A limitation of this principle is that transit time is a spatially and temporally heterogeneous quantity, but that this is not captured in the standard formulation of the CVP. In this Chapter, the central volume principle is therefore:
  - extended to account for spatial heterogeneity in the distribution of blood vessel volumes in the brain, and
  - related to an ODE that expresses transit time as a quantity that itself varies with time
- Chapter 4 examines the application of an enumerative sampling plan with a fixed level of precision, based upon the pioneering methods of Kuno [4] and Iwao [2], to designing fMRI studies.
- Chapter 5 treats a similar problem to Chapter 4, but evaluates the accuracy and precision of fixed size sample plans. Implications for the optimal design of fMRI experiments are discussed.
- Chapter 6 considers the model for transit time from Chapter 3 from a probabilistic perspective, and examines the effect of oxygen utilisation by the brain on the results of the preceding chapters. First, the ultimate fate of a single oxygen particle having a given transit time is explored from a general probability. Subsequently, the behaviour of this particle is linked to the state of other oxygen particles using stochastic simulations. Implications of the findings for fMRI models are reviewed.

- Chapter 7 reviews the findings of the thesis, and discusses avenues for future work.

In summary, the thesis makes several new contributions, each contained in a Chapter:

- In Chapter 3, the CVP is extended to account for spatial heterogeneity, and related to a differential equation expressing it as a time-dependent quantity.
- In Chapter 4, the application of enumerative sampling methods in fMRI is assessed based on fitting to experimental data.
- In Chapter 5, simulations of fixed sample size plans are used to derive operating characteristics for fMRI studies.
- In Chapter 6, the effect of oxygen utilisation by the brain on the previous results is examined using stochastic simulation.

Chapter 2

Literature review

2.1 Principles of neuroimaging relevant to the haemodynamic response function

There has been considerable interest, both academic and public, in the research findings from the field of neuroimaging.[5, 6] In particular *functional magnetic resonance imaging*, fMRI, has been applied as a research tool in a wide range of circumstances. Its suitability for use in the health sciences and psychology is due to its noninvasive properties, and purported ability to produce near real time images of brain function.[7] The research findings range from diagnosing and understanding neurological disease, discovering novel insights into the mechanical properties of cortical connectivity, and understanding correlations between psychological behaviour and localised brain activity.[7, 8] Since its humble beginnings in the 1990s, fMRI research has become one of the fastest growing fields in the medical sciences [6], in particular in neuropsychological research. The primary purpose of any neuroimaging experiment is to provide a map of either the structural properties of brain tissue or the functional aspects of different cortical regions localised to specific tasks.[9] The hopes and prospects of what this technology might achieve has at times appeared to be

overestimated within public perception and underestimated by critics of the field.[10] Due to both professional and public confidence in the ability neuroimaging to explain the how the brain works, it is important for researchers in the field to investigate where improvements in the physiological and mathematical models for the technology can be made.[11, 10] For the field of neuroimaging to achieve this, it must improve its understanding of what neuroimaging can in fact do and how well can it do it.[12] This thesis is an attempt to contribute to the growing body of literature that is in search of improving the mathematical models that underpin the subject to produce more reliable results for experimenters and clinicians.

2.2 Who is interested in neuroimaging and why?

Neuroimaging research is frequently referenced in the media and used in a wide variety of contexts, such as criminal law cases and public policy.[12, 13] It has become the primary experimental tool for clinicians and theoreticians in fields broadly labeled under the banner of cognitive neuroscience. The foundation disciplines that were at the beginning of the field are computer science, medicine, neuroscience, psychology and psychiatry.[14] Students of neuroimaging will be required to study physics, engineering, computer science, statistics, medicine, neuroscience, mathematics, chemistry, and physiology.[7] But, today, researchers in public policy, behavioural economics, political science, law, sociology, philosophy, and even theology are also interested in the results of fMRI experiments. Public confidence that fMRI has implications for discerning between the sick and well, the sane and insane, the mad and bad, are strikingly optimistic, but the history of science has demonstrated that the importance of scientific disciplines as young as neuroimaging can often be overstated. A much noted example of this foolhardy approach were the undelivered promises of phrenology, invented in the 19th century by Franz Joseph Gall and J. G. Spurzheim.[14] Their technique called *anatomical personology* correlated protrusions in the cranium to a set of psychological attributes.[14] It was thoroughly discredited early in the 20th century, but still had naive

supporters well into the latter half of the century. Finding a balanced perspective on the possible benefits and limitations of fMRI can be said to be an obstacle to understanding the importance of the research field as a whole, and to communicating the results of fMRI research to a plethora of interested groups. The aim of this thesis is to analyse and improve existing mathematical models of the haemodynamic response to stimulation HRF, which underpin fMRI research, and to discuss the relevance of these to clinicians and researchers in the field.

2.3 Why the focus on fMRI in particular?

fMRI detects the *blood oxygenation level dependent*, BOLD signal, using large magnets in a scanner, which is a representation of the underlying physiological properties of the HRF.[7] The assumption in fMRI experiments is that neural activity responds to a range of environmental and internal stimuli that cause changes in the physiological activity of the brain, demanding a surplus of blood to flow to particular region of the brain, each known as a *region of interest*, (ROI).[15] Researchers using the fMRI modality assert that a central focus in fMRI research is that the local cerebral metabolic rate of oxygen ($CMRO_2$), the rate at which oxygen is perfused into the nervous tissue for metabolic demand, increases between 10-30 % in response to stimulation.[16, 17] But the regional cerebral blood flow (CBF) increases by 20-80% during stimulation.[18, 16] This uncoupling of the $CMRO_2$ and CBF rate leaves a ratio larger than unity.[17] The excess of oxygenated blood produced by this process is known as hyperemia, and this is what neuroimaging aims to detect.[17, 7] This difference between supply and demand is called the BOLD signal, or contrast. Unfortunately, the mathematical relationship linking the BOLD signal and HRF is not completely understood. Understanding this relationship is important for being able to model the correlation between neural activity and the true underlying HRF. The idea of a correlation between neural activity and changes in blood distributions in the body dates back as far as William

James, the Father of American psychology from the 19th century.[19] Researchers are now confident that we can attribute specific neural activity categorically to different stimuli with discretely localised cortical activity.[20] The intensity and detectability of the relationship between BOLD and HRF varies according to the phenomena being investigated. Responses detectable by fMRI can be observed with motor and sensory neuronal activity, but there is less confidence that fMRI accurately detects changes in the areas of higher order processing and cognition.[8] The pioneering discoveries in the latter half of the 20th century, by Paul Lauterbur, Peter Mansfield, and Raymond Damadian, regarding the detectable magnetic properties of hemoglobin molecules that travel in the oxygenated blood allowed for the possibility of measuring the behaviour of the HRF and converting them into useful images, via the BOLD signal.[21] Specialists in fMRI are aware of the multifactorial nature of underlying variability in the BOLD. One apparent cause of variability is noise in the signal arising from artifacts in the design and experimental tools. But, more importantly, there are reasons to believe physiologically the primary reason for changes in the HRF are not just a response to neural activity. The functional properties of the brain are not just subject to cognitive processes, but also to physiological systems such as the endocrine, immune, circulatory, muscular, and neuroendocrine.[11] So it is important to question the assumption of the causal link between the HRF and neural activity.

The importance of fMRI to produce invaluable structural images for the diagnosis of brain abnormalities detectable in white and gray matter must not be dismissed.[11][1] Further, the functional aspects of fMRI imaging are providing insights into the complicated networks, or neural connectivity, involved in rudimentary cognitive tasks. But, it is important to scrutinise what claims and assumptions are held by the field, in order to make progress. This will

[1] Other imaging modalities that utilise this feature of brain activity are: PET, aslfMRI, EEG, and CAT, see list of abbreviations in appendix 1

involve raising questions about theoretical notions such as the nature of blood flow through the brain.

2.4 The assumptions of the physiology behind the BOLD

The HRF itself is mathematically a black box. This is not to say any extraordinary discoveries have yet to be made, but rather that any predictability in its behaviour is not understood at a fine grain level, because inputs are not easily related to outputs.[22] There is still much to learn about the nature of the brain from a wide range of perspective and disciplines ranging from the scale of the suba-atomic to the macroscopic.[23] Original hopes within the fMRI community to understand the mathematical relationship of neural activity to the HRF, via the BOLD signal, as a simple "unitary entity"-a simple deterministic function-have turned out to look like a pipe dream.[24] Instead, a complicated dynamic relationship is the only way to connect the numerous features of the cerebral cardiovascular system that make up the HRF and what is produced as cognitive output. The BOLD signal is determined by three fundamental parameters: the *cerebral blood volume* (CBV)-the amount of blood present in a vessel, *cerebral blood flow* (CBF)-the volume of blood flowing through a vessel per minute, and the *cerebral metabolic rate of oxygen* $CMRO_2$-the rate of oxygen molecules to be metabolised.[25] The relation between the $CMRO_2$ to CBV is relatively straight forward to model.[24] The important physiological process that the BOLD actively relies on capturing is the relationship between the CBF and $CMRO_2$.[26] This is dependent on the discovery of the “uncoupling” phenomena.[27] The resting state measurements of the two variables show a large positive correlation (.87), but this changes when neural stimulation is involved.[27] To account for this unexpected change the oxygen extraction fraction(OEF) must be factored into the models.[16] This is a rate constant that implies that if one variable increases the other must decrease in turn.[28] But the OEF depends upon a principle in physiology called the *central volume principle* (CVP). The CVP assumes that changes in transit times of oxygen

particles in the blood are determined by the ratio of blood vessel volume to blood flow, with blood leaving the heart in larger volume vessels, and passing through major organs, including the brain, in smaller volume vessels. The CVP is the foundational equation for measuring the travel time of a particle *region of interest* (ROI) in the cardiovascular system [25, 29], and is given by

$$\bar{t} = \frac{\mathrm{V}(ml)}{\mathrm{F}(ml/s)}, \tag{2.1}$$

where $\bar{t}$ is the mean transit time of an oxygen particle; V is the blood volume in ml; F is the blood flow rate (ml/s). We now understand, however, that cerebral blood flow is governed by different mechanisms than blood flow in the rest of the body. In most of the body, constriction of blood vessels is the primary regulatory mechanism, but the brain has different demands and regulation of blood flow. This means that the status of the CVP as a building block of fMRI models needs to be reassessed.

The brain relies on a constant supply of oxygenated blood, which turns out to consume over 20% of the heart's cardiac output, making the constant regulation of blood supply to the brain a necessary feature of the cardiovascular system .[17, 30] It follows from this that the brain as whole must have a relatively constant rate of blood flow to avoid neurological damage, stroke, or death of the organism.[30] This further entails at times where there is an increase in metabolic demand, there is an increase in mean transit time.[24] The question might be posed, could certain systems of arteries to and within the brain provide vascular resistance necessary to segment the flow to appropriate areas of the brain without demanding an increase in overall transit time of blood flow?[30] If this was the case, it would increase the mean transit time to a smaller region (see eqn. (2.1)). Some authors propose there are mechanisms to maintain uniform transit times, such as the theory that the parenchymal arterioles with significant basal tone, play a significant role in controlling this flow.[30] This

in turn raises the question, how many processes are involved in changes in transit times of blood flow? Further, what role do the different vessel types that constitute the cerebral cardiovascular system play in the changes and regulation of transit times? The biophysical understanding we have of the relationship between hyperemia and metabolic demand are directly related [17], but what causes the metabolic demand needs to explored further. The early models of the uncoupling phenomena in [16] assume that extraction of oxygen is the same across all regions of the brain.[16] If this is true and different regions of the brain have different demands for oxygen, how can this requirement be met? This is the central question motivating this study.

Linking (2.1) to experimental data has always proven difficult.[2, 31, 19] Theoretically, the equation allows a researcher to estimate the value of any one of the three parameters where the other two are known.[25] Unfortunately, values for the blood flow parameter are exceedingly difficult to obtain experimentally.[25] Therefore, parameterisation of the equation has always relied on measures of blood vessel volume and transit time derived from imaging techniques[25], or the use of indicator dyes, the latter of which has been used for over a century.[31] Unfortunately, estimates of these parameters used in fMRI research have been derived from areas outside the brain (such as transit times through the external jugular vein), or from animal models using different technologies such as PET scans.[27] The question needs to be asked: does the failure (so far) of fMRI technology to deliver the kind of results expected by experts and the community relate to problems with the foundational models used to understand experimental results?

In this thesis, the foundational CVP model is reexamined in light of new physiological evidence, and revised. Implications of the revised model for understanding fMRI research

are then examined. Finally, the effect of the uncoupling phenomenon on transit times is reinvestigated using stochastic simulations.

Chapter 3

Modelling the transit time of a particle through a vascular pathway

3.1 Introduction

As described in the preceding chapter, a foundational assumption of fMRI models is that the mean time for an O_2 molecule to pass through a blood vessel in the brain is described by the central volume principle (CVP). The CVP relates the volume of a vessel and the flow rate of blood to the transit time of a molecule, but typically assumes that both volume and flow are spatially and temporally homogeneous physical properties of blood vessels. In fact, as shown in this chapter, the model typically advanced for the CVP assumes homogeneity of vessel volumes. This is clearly unrealistic. This chapter will reconsider the dynamic relationship between the three parameters of the CVP, blood flow F, blood volume V, and transit times $\bar{t}$, and propose a modification to the CVP that no longer requires that these key parameters are spatially and temporally homogeneous. As the foundational differential equation models in fMRI are based on the traditional form of the CVP, any modifications to the principle will have implications for experimental research. The implications of the

modified CVP developed in this chapter for the analysis of fMRI experiments will therefore also be considered.

3.2 Relation of the CVP to foundational experimental models

The traditional CVP is given by the previously described equation (reprinted here for convenience),

$$\bar{t} = \frac{V}{F}, \tag{3.1}$$

in which $\bar{t}$ is the mean transit time of an O_2 molecule, V the tissue volume occupied by blood vessels, and F the flow rate in these. The importance of the CVP to fMRI modelling arose as a consequence to early experiments that applied the CVP, (3.1), to animal experiments on the general circulation.[32] Early fMRI modellers then applied this equation to modelling transit through an idealised conception of the brain's circulation.[33] More recently, it has come to be understood that the brains circulatory system (in particular regulation of blood flow) is different in some ways to that in the rest of the body. This turns out to be important, as there are some distinct differences in the conceptual model of [33] and the principles governing the experimental models.

The foundational experiments of [32] relied heavily upon fundamental principles of fluid mechanics in constructing their hypothesis of how a substance might be carried through the bloodstream. In particular, the experimental design assumed that the principle known as Fick's first law was true of the circulation. If true, when two miscible liquids (an indicator solution and blood) were combined by injecting the indicator, the indicator would move

macroscopically from areas of high concentration (the injection site) to areas of low concentration (the rest of the vasculature).[34] In essence, the experiments assumed that the vascular system of the experimental model was a jar of liquid through which another concentrated liquid would diffuse predictably. Hence, after injecting indicator at one site, after a period of time (governed by the diffusion rate) had passed, the indicator would be measurable (at lower concentration) at some other site in the system. The (3.1) models the time required for a particle to move between its initial and final position in such a system, as was demonstrated by [32].

Early fMRI models employed the concept of the vascular bed as an attempt to develop an idealised mathematical system that applied the above model to the transit of an oxygen particle through the brain.[33] The vascular bed was defined as a "black box", meaning that it was a system of vessels with one entry point for a particle and one output point for a particle, but the arrangement of vessels between these points was unknown and seemingly unknowable. At this time, there existed some empirical estimates of transit time through the brain, meaning that volume and flow through the vascular bed could be chosen for (3.1) to yield the required value of $\bar{t}$. This was a reasonable model for a system with one input, one output and an arbitrary volume in between. However, later on in the paper (p. 400, [33]) claimed that (3.1) was applicable to a far more general set of circumstances; specifically, he claimed that if the arrangement of vessels between input and output was known, and that if either more than one input or more than one output was permitted, that the expected transit time of a given particle would still be described by (3.1). This statement became the basis for the reliance on (3.1) to model the transit time of oxygen particles in most fMRI models.[28] In this chapter, the claim that (3.1) applies to any system of vessels in any arrangement is now re-investigated. Ultimately, it is shown that the CVP as expressed in (3.1) relies upon homogeneous blood vessel volumes. First, this is demonstrated by examining a simple system comprising two

blood vessels. Then, conclusions from this simple case are generalised to more complex scenarios. Finally, a different version of the CVP accommodating these results is then developed.

3.3 The traditional CVP requires homogeneity of vessel volumes

3.3.1 Simple worked example: a system of two blood vessels

Essentially, there are only two ways to arrange a system of two blood vessels or two vessel segments: in parallel, where the movement of particles in one vessel is independent of the movement of particles in the other; or in series, i.e. joined together, so that flow out of one vessel goes into the other. In the second possible arrangement, the movement of a particle in each vessel or segment is not independent of its movement in the other, as once joined together the vessels function as one unit. By applying Fick's first law to these two scenarios, six biologically and physically possible combinations of volume and flow parameters can be identified. These six cases are enumerated in Table 3.1, and equations are now derived from first principles showing how the indicator-dilution principle would operate for these systems in practice. It is then shown which of these cases correspond to the standard interpretations of the CVP (3.1) and to our current understanding of the physiology of the vessels.

Table 3.1 Possible combinations of flow and volume parameters in systems of two vessels.

Case	Flows	Volumes	Vessel relationship
I a)	$F_1 = F_2$	$V_1 = V_2$	Parallel
I b)	$F_1 = F_2$	$V_1 = V_2$	Series
II a)	$F_1 = F_2$	$V_1 \neq V_2$	Parallel
II b)	$F_1 = F_2$	$V_1 \neq V_2$	Series
III	$F_1 \neq F_2$	$V_1 \neq V_2$	Parallel
IV	$F_1 \neq F_2$	$V_1 = V_2$	Parallel

Considering case (Ia) from Table 3.1, when two vessels of equal volume are filled with a fluid at a constant flow rate, the mean time for a particle of some dissolved substance to transit the system has an expected value of

$$\bar{t} = \frac{2V}{2F}. \tag{3.2}$$

Thus the CVP, (3.1), applies for systems arranged according to case I a).

Case (II a) is similar to case (Ia), except it considers the more likely scenario that the volumes of the vessels or vessel segments in the system are different, but that blood flows through the system at constant rate. For this case the expected transit time of a particle through the system would correspond to the mean volume of the vessels divided by the flow,

$$\bar{t} = \frac{V_1 + V_2}{2F}. \tag{3.3}$$

This case, as well as (3.2), which is the simplest case of (3.3) can easily be extended to systems of n vessels, in which case (3.3) will approximate (3.1) as $n \to \infty$. Thus it is clear that the CVP applies perfectly to systems of n independent vessels of equal volume receiving a constant flow, and in the large limit as an adequate mean field approximation for systems

of n heterogeneously sized independent vessels receiving constant flow. The importance of the assumption of independence in these cases cannot be overstated; so far, we have only demonstrated that the CVP holds where there is an equal probability of a particle transiting through any vessel. This assumption is unrealistic, for reasons which will be explored more fully later in this chapter.

Considering now cases I b) and II b), where vessels are joined, it becomes clear that (3.1) works less perfectly in these systems. Systems of joined vessels are more realistic as a model of the transport of substances through the cardiovascular system than are systems of vessels in parallel. This is because the route that a particle of some substance takes through the body is a path originating from and returning to the heart. Initially the path is made up of arteries of large diameter, which take blood away from the heart. As the particle is transported further from its origin, it passes through smaller and smaller vessels, until it eventually reaches a capillary, which is approximately one red blood cell in diameter. After the capillary sized vessels, the vessels making up the path begin to progressively increase in diameter, until they almost equal or surpass the first arteries leaving the heart in diameter. It is through these very large veins that the particle will return to the heart.[1] Thus, the case of joined vessels (in nature, almost always of different volumes) is very important biologically .[28, 35]

In order to model the passage of a particle through vessels in series, equation (3.2) must be modified. Considering case Ib), were two vessels of equal volume joined together, and fluid passed through them at constant rate F, the expected value of the transit time would

[1]This representation of a path through the body assumes for the present that the particle is not extracted from the vascular system for use in the metabolic processes of an organ. The effect of extraction of particles on the state of the system is examined in Chapter 6.

now be

$$\bar{t} = \frac{2V}{F}. \tag{3.4}$$

In other words, as is intuitively clear, the time taken for a particle immersed in the fluid to transit two of these vessels would be double that required to transit just one. Clearly, (3.4) is not equivalent to (3.1). Therefore, the CVP does not apply to systems of joined vessels of equal volume (corresponding to case I b) in Table 3.1) in its usual form. Extending (3.4) to account for joined vessels of different volumes, corresponding to case II b) in Table 3.1, the expected transit time of a particle becomes

$$\bar{t} = \frac{V_1 + V_2}{F}. \tag{3.5}$$

Eq. (3.5) gives the general form of (3.4), but is also clearly not equivalent to (3.1). Therefore, the CVP does not apply to systems of joined vessels in its original form. There is also an intuitive realism to the interpretation of (3.5) that is absent when considering equations such as (3.3). The realism is that when vessels are joined together, it must take a particle longer to transit through them. Unfortunately, in (3.3), the more vessels that are present in the system, the quicker (on average) a particle moves through the system. In other words, it takes a particle a shorter time to move through one of two vessels that are arranged in parallel than to move through a single vessel. This clearly makes little sense biologically or mathematically.

Putting aside the mathematics for a moment, a possible biological criticism of the claim that (3.5) is a superior model of transit time to the CVP given in (3.1) exists. This criticism is that, in reality, blood vessels are arranged both in series and parallel within the body, as shown in Fig. 3.1. This is certainly true anatomically, but arguably the appropriate mathematics for studying this system are still those in (3.5). This is clear when one considers the fate of a

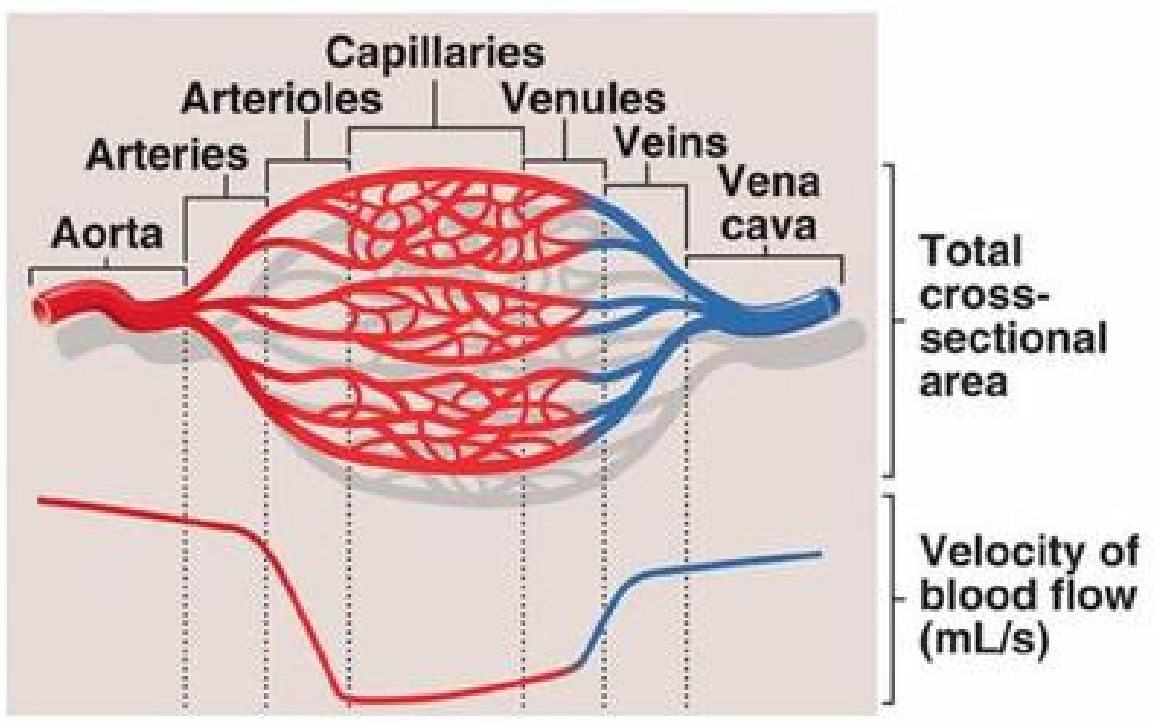

Fig. 3.1 Illustration of the network of vessels making up the cardiovascular system for oxygen transport through the brain. The figure shows that the vasculature are biologically constitutive of the structural apparatus of parallel and series models of blood flow. Available at https://www.pathwayz.org/Tree/Plain/BLOOD+VESSELS

single particle moving through the body. A single particle can only take one pathway through the cardiovascular system; it cannot be in more than one place at one time. The existence of multiple possible pathways through vessels arranged in parallel affects the probability of taking a particular path, but not the time taken to pass through it. This topic is covered in more detail in the next chapter of the thesis. Furthermore, the pathway through organs close to the heart (for example, the lungs) is much shorter than the pathway through an organ far from the heart, such as the big toe. It is clear that all else being equal, it will take much longer for a particle to travel to the big toe than to the lung, or indeed to the heart muscle itself. Only (3.5) gives a longer expected transit time for a longer versus a shorter system of joined vessels of different sizes. Therefore, (3.5) is the best model for the transit time of a particle through the body. It is this equation that will form the basis of more complex models

of oxygen transport developed in the rest of this thesis.

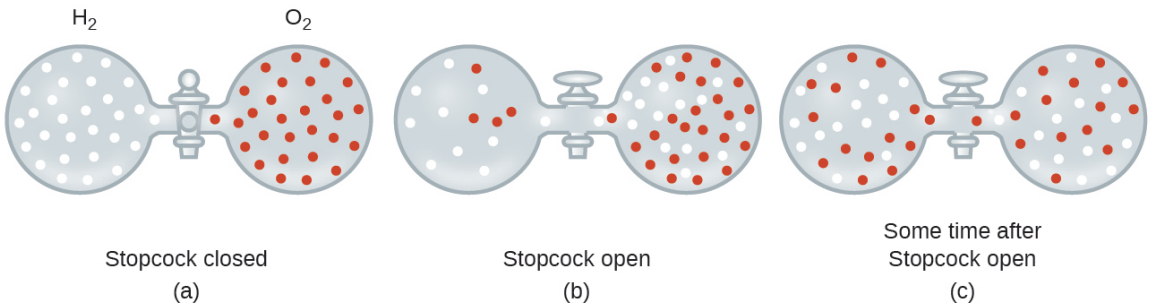

Fig. 3.2 Example of particle diffusion through a container. This indicates that the distribution of particles in the vessels will diffuse throughout entire available space. Available at https://bit.ly/2Q9ySRl

3.4 Modelling the transit time of a particle through a path of different blood vessel types

Having demonstrated that (3.5) is a better model than (3.1) for transit time through a system of heterogeneously sized vessels joined together, transit time through a spatially and temporally heterogeneous vascular system is now modelled as a function of time. Transit time may vary with time for a range of reasons (gravity, collisions between particles, change of volume of elastic vessels, etc.)

Spatial heterogeneity is introduced by modelling heterogeneous volumes of blood vessels at multiple levels. First, the total volume of the vasculature, V_T is expressed as the sum of the total volumes occupied by different types. This is given by the equation,

$$V_T = V_A + V_a + V_c + V_v + V_V, \tag{3.6}$$

where V_A is the volume of the arteries; V_a is the volume of the arterioles; V_c is the volume of the capillaries; V_v is the volume of the venules; and, V_V is the volume of the veins. Each type of vessel is further divided into individual vessels of different volumes, such that

$$V_q = V_{q_1} + V_{q_2} + \ldots + V_{q_n} \tag{3.7}$$

for the q^{th} vessel type. If it is assumed that the pathway that a single particle of indicator or oxygen takes through these vessel types is made up of just one vessel of each type, the expected volume of vessels it passes through can be expressed as

$$E(V_T) \sim \bar{V}_A + \bar{V}_a + \bar{V}_c + \bar{V}_v + \bar{V}_V. \tag{3.8}$$

For each volume term $\bar{V}_q$ in (3.8), there exists a corresponding expected transit time through vessel type q, $\bar{t}_q$, derived from (3.5). For example, the expected capillary transit time would be given as,

$$\bar{t}_c = \frac{\bar{V}_c}{F}. \tag{3.9}$$

Applying the improved model for joined vessels of different volumes, (3.5), to equations (3.8) and (3.9) yields the net total expected transit time across all vessel types, $\bar{t}_T$, as

$$\bar{t}_T = \frac{\bar{V}_A + \bar{V}_a + \bar{V}_c + \bar{V}_v + \bar{V}_V}{F} = \sum_{q}^{Q} \bar{t}_q. \tag{3.10}$$

Thus, the expected transit time of a particle through a system of vessel types is the sum of the expected transit times through the individual vessel types. The distribution of mean transit times will be determined by the proportion of vessel types that comprise the system a particle traverses. This continuous distribution will fall between the lowest value, where the proportion of vessels consists entirely in the capillaries, $(\forall V_q : V_q \in V_c)$, and a maximum

value, where the entire proportion of vessels contain arteries, $(\forall V_q : V_q \in V_A)$.[29, 31] The pathway for a particle through only the largest and smallest vessel types can be modelled using the step function

$$\bar{t}_q = \begin{cases} \frac{\bar{V}_{max}}{F} & \forall V_q : V_q \in V_A \\ 0 & \forall V_q : V_q \in V_c. \end{cases} \tag{3.11}$$

Using the extreme values from (3.11), it can be shown that the mean transit time is related to the maximum transit time by a logistic curve if:

1. The mean value is half of the maximum.
2. At half the maximum value of the function, the value of second derivative is equal to zero, indicating that a point of inflection occurs there.

Therefore, let the relationship $\bar{t}_q = f(\bar{V}_q)$ be described by

$$f(\bar{V}_q) = \frac{\bar{t}_{max}}{1 + Ae^{-F(\bar{V}_q - 0)}}, \tag{3.12}$$

where, $\bar{t}_{max}$ is the limit; F the steepness of the curve, given by the flow rate; and A is a positive integer to represent the starting point of the curve.

The inflection point for the logistic equation (3.12) is found solving the second derivative for zero. The second derivative is

$$f(\bar{V}_q)'' = \frac{(-AFe^{-F(\bar{V}_q)})^2 - (AF^2e^{-k(\bar{V}_q)}}{2\bar{t}_{max}(1 + Ae^{-F(\bar{V}_{max})})^3 \bar{t}_{max}(1 + Ae^{-F(\bar{V}_{max})})^2} \tag{3.13}$$

and the value of $\bar{V}_q$ when the second derivative is zero is

$$\bar{V}_q = \frac{lnA}{F}. \tag{3.14}$$

Substituting into (3.11),

$$f(\frac{lnA}{F}) = \frac{\bar{t}_{max}}{1+Ae^{-F(\frac{lnA}{F})}}$$
$$f(\frac{lnA}{F}) = \frac{\bar{t}_{max}}{2}. \tag{3.15}$$

The mean value occurs at half of the maximum value of the function, and at this point the second derivative is equal to zero. Therefore, the relationship between transit time and volume is logistic.

The distribution of possible transit times measured at different times, Δt, is also modelled using a logistic function, by similar argument. The smallest difference between transit times measured over the interval Δt is equal either to 0, or the largest difference t_{max}. Let the total transit times as a funtion of time be described by

$$t_T(t) = \frac{r}{e^{-rt}+h}, \tag{3.16}$$

which has a maximum value of r/h. The second derivative of (3.16),

$$t_T(t)'' = t_T(t)'r - 2ht_T(t)) \tag{3.17}$$

equals zero at

$$t = \frac{-lnh}{r}. \tag{3.18}$$

Substituting (3.18) into (3.16) gives,

$$t_T(\frac{-\ln h}{r}) = \frac{r}{e^{-r(\frac{lnh}{-r})} + h} \tag{3.19}$$
$$t_T(\frac{-\ln h}{r}) = \frac{r}{2h}.$$

The second derivative of (3.16) equals zero (the inflection point) when the value of the function is half the maximum; thus, transit time as a function of time can be described using a logistic function.

It follows that the difference in transit time as a function of time can be modelled using the first derivative of (3.16), which is

$$\frac{dt_T}{dt} = t_T(t)(r - ht_T(t)). \tag{3.20}$$

Biologically, the parameters of the logistic equation (3.20) can be interpreted as follows. The parameter r is the deceleration of a particle from its initial velocity. The parameter h gives the effect of more and longer pathways on transit time.[2] These parameter interpretations are best understood by recalling that a transit time approaching zero[3] is very fast (equivalent to the time taken to pass through the capillaries according to [32]), and a large value represents a long transit time. Henceforth, the (t) notation is omitted for clarity of presentation, but note that transit time variable remain functions of time.

[2]If the electrical circuit analogy introduced previously for systems of vessels in series and parallel is continued with, carrying capacity can be considered similar to "capacitance".

[3]A transit time of exactly zero can be taken to indicate no movement occurs; this will be explored more in the next chapter

3.4.1 Application of the transit time model to oxygen transport in the brain

Compared to a relatively linear path that does not differ much between individuals, such as through the femoral arteries and veins, the path that a particle may take through the brain is very torturous, differs substantially between people, and traverses substantial and complex networks of capillaries. For application to such a system, (3.20) needs to be generalised to apply to any number of vessels, of any volume, and of any type (arteries, capillaries, etc.). To generalise (3.20) to account for differences in transit time across Q vessels of different types in the brain, (3.20) can be rewritten as

$$\frac{dt_T}{dt} = \sum_{q=1}^{Q} t_q(r - ht_q), \tag{3.21}$$

with t_T denoting the total transit time through the brain. The introduction of Q vessels into the deterministic model allows for measuring the effect of the change in any vessel q's volume over time on the transit time of a particle. In the brain, a substantial proportion of vessels are capillaries. As established by [32], transit time through capillaries is so rapid that the time to pass between two points in a capillary can be considered equal to zero. Distributions of values featuring a large number of zeros are called overdispersed, and it is has been shown previously that logistic equations such as (3.20) and (3.21) require modification to accurately model overdispersed quantities.[1] Following [1], I incorporate a distance measure by dividing (3.21) by $\sum_{q=1}^{Q} t_q$, which expresses the transit time through each vessel as a function of the transit times for all vessels.

Obtaining

$$\frac{1}{\sum_{q=1}^{Q} t_q}\frac{dt_T}{dt} = r - h\frac{\sum_{n=1}^{Q} t_q^2}{\sum_{n=1}^{Q} t_q}, \tag{3.22}$$

note that the term,

$$\frac{\sum_{q=1}^{Q} t_q^2}{\sum_{q=1}^{Q} t_q}, \tag{3.23}$$

is mathematically equivalent to Lloyd's mean crowding index [3],

$$x^* = \frac{\sum_{q=1}^{Q} x_q^2}{\sum_{q=1}^{Q} x_q} - 1, \tag{3.24}$$

plus one. The mean crowding index is mathematically simple but has profound implications for understanding the behaviour of dynamical systems .[1] The terms crowding, overdispersion, and aggregation are used interchangeably in relevant literature, because where observations in a data set cluster, it is expected that there are relatively more observations that equal zero. Essentially, mean crowding is a way to account for the effect of such overdispersion on estimates of mean behaviour.

The mean crowding index, has an alternative and equivalent formula that expresses it as a function of the first two moments of any probability distribution. For any distribution, where $\bar{x}$ and s^2 are considered the first and second moments of the distribution, mean crowding can be as expressed as

$$x^* = \bar{x} + \frac{s^2}{\bar{x}} - 1 \tag{3.25}$$

This formulation has the advantage of linking (3.24), which describes mean crowding in terms of a set of empirical measurements, to the parameters of a number of probability distributions explicitly.[2] Moreover, it can be shown using (3.25) that mean crowding has a

Table 3.2 Values for a a and b for given transit times for oxygen particles diffused in blood

Distributional assumptions	b	a
Uniformly distributed variable	1	-1
Distribution of variables is regular (underdispersed) but not uniform	$0-1$	-1
Poisson distributed variables	1	0
Poisson distributed clusters of variables	1	>0
Overdispersed (negative binomially) distributed variables	>1	0
Overdispersed distributed clusters of variables	>1	>0

linear functional relationship with the mean.[2] Consider a linear equation of the form

$$x^* = a + b\bar{x}. \tag{3.26}$$

Values of a and b that link x^* to the mean of a number of probability distributions are shown in Table 3.2. How these values are derived is best seen by considering (3.25) and (3.26). For example, for a Poisson distributed random variable $s^2 = \bar{x}$, so it can be seen simply that $x^* = \bar{x}$ for both (3.25) and (3.26). The statistical definition of an overdispersed distribution is one where $s^2 > \bar{x}$, so $x^* > \bar{x}$. For both (3.25) and (3.26) to satisfy $x^* > \bar{x}$, requires either $a > 1$, $b > 1$ or both. Hence, it is easy to see how the parameters expressing mean crowding in terms of a and b can be used to model the effect of different probability distributions on the expected mean value of some quantity.

Returning to the transit time model from (3.22), the presence of the mean crowding term means that different distributions of vessels can be included by substituting the linear relationship of variance and mean for (3.23). Recalling that (3.23) is equivalent to mean

crowding ((3.24)) plus one, (3.22) can be rewritten as

$$\frac{1}{\sum_{q=1}^{Q} t_q}\frac{dt_T}{dt} = r - h(t_T^* + 1), \tag{3.27}$$

where $t_T^*(t)$ is the mean crowding of transit times for any time point. Equation (3.27) can be further written in terms of the linear relationship between $t_T^*(t)$ and the mean $\bar{t}_T$, giving

$$\frac{1}{\sum_{q=1}^{Q} t_q}\frac{dt_T}{dt} = r - h(a + b\bar{t}_T + 1). \tag{3.28}$$

As $\sum_{q=1}^{Q} t_q = t_T$, (3.28) can be rewritten as

$$\frac{dt_T}{dt} = rt_T - h(a + b\bar{t}_T + 1)t_T \tag{3.29}$$

It is apparent from (3.29) that different values of parameters a and b have considerable effect on transit time. The conventional CVP does not allow for this analysis and leaves itself open to error in estimating transit time in overdispersed systems of vessels, where the variance is significantly larger than the mean. As shown in Table 3.2, (3.29) can do this, whilst being equivalent to the improved CVP-type relationship given in (3.5) and (3.10).

Equation (3.29) has two equilibrium solutions: the trivial solution 0, and

$$\bar{t}_T = \frac{\frac{r}{h} - a - 1}{b}; \tag{3.30}$$

the notation $\bar{t}_T$ is used, as (3.30) will correspond to the average value of transit time in a system at equilibrium. It is straightforward to show that for $r < h(a+1)$, the trivial solution of (3.29) is unstable and the positive solution (3.30) is stable. The converse is true for $r > h(a+1)$. Biologically, the interpretation of these results is subtle; recall that previously

it was noted that whilst a transit time of *almost 0* is taken to be very fast, a transit time of *exactly 0* is taken to mean no movement at all. The interpretation of the stability conditions is therefore that for the particle not to move at all between two points, or a transit time of exactly 0, deceleration needs to be very large in value. Conversely, for a positive non-zero value of transit time to be the equilibrium solution to be stable, deceleration r must be less than the "capacitance" of the system h. This is best understood by thinking that is deceleration is low, the particle remains close to its initial velocity in its value. In a sense, transit time is described by a step function; there is no transit time if there is no movement ($t_T = 0$), or else the particle does move between two points, but decelerating slightly as t_T increases. The implications of these results for transit time with different distributions of vessel volumes are now shown numerically.

3.4.2 The effect of heterogeneous blood vessel volumes on transit time: Numerical results

The effects of different distributions of vessel volumes on maximal transit time were analysed numerically. Numerical analysis used Euler's method to approximately solve (3.29). Initial conditions were $t_T(0) = 0.0001$, and parameter values common to all simulations were $r = 0.167$ and $h = 0.025$. Values of a and b for three different distributions of blood vessel volumes (uniform, Poisson and overdispersed) corresponded to those in Table 3.2. The results showed that overdispersed distributions of vessel volumes significantly decreased transit time, as shown in Figure 3.3. Taken in concert with the analytical results previously outlined in this chapter, this finding has clear implications for interpreting the clinical implications of existing fMRI models, as discussed below.

Table 3.3 Equilibrium values of (3.30), given parameters describing different distributions of blood vessel volumes.

Parameters	Equilibrium transit time	Distribution of blood vessels
$a = -1, b = 1$	$\frac{r}{h}$	Uniform
$a = 0, b = 1$	$\frac{r}{h} - 1$	Poisson
$a \geq 0, b > 1$	$\frac{r}{h} - 1$	Overdispersed

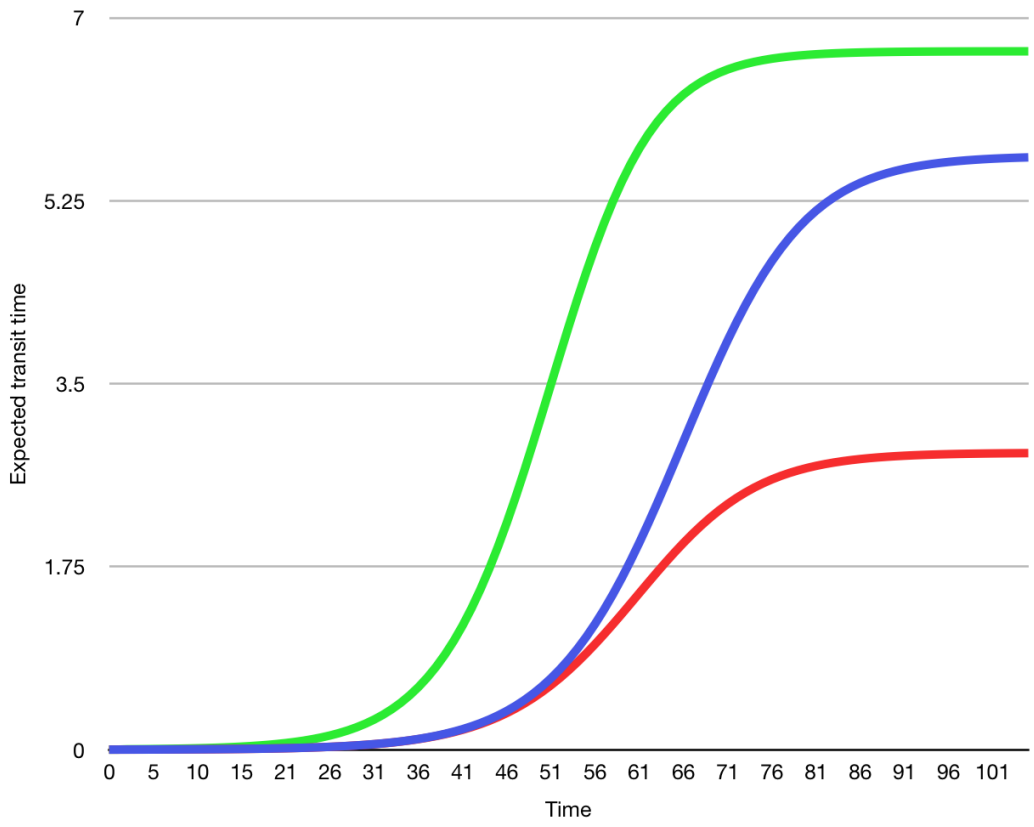

Fig. 3.3 Numerical solutions to (3.29) for three different distributions of vessel volumes.

3.5 Discussion

In conclusion, this chapter set out to examine the assumptions of the standard interpretation of the CVP in relation to modelling the hemodynamic response function. It was found that it relates the blood volume and flow of system of vessels as homogeneously distributed. This does not reflect the anatomical realities of blood vessel distribution. A different formulation of the CVP was suggested to account for the different formations that blood vessels may take. The analysis provided a more suitable framework for extending the (3.2) into a differential equation capable of determining the effect spatial heterogeneity has on transit times, given specified distributions of blood vessel volume.

This chapter makes a number of contributions to the study of the transit time of oxygen particles through the brain. First, this chapter demonstrated that the conventional CVP (a building block of fMRI modelling, given in (3.1)), only holds for a system of homogeneously distributed blood vessels, that run in parallel. Such a system is similar to the idealised vascular bed used by [29], but displays a number of unrealistic properties. For example, transit time always decreases in this model as the total volume of vessels passed through decreases, due to the assumption of a parallel network of vessels. This is not realistic, as in the body, many vessels are joined in series, and it will take longer for a particle to pass through two vessels arranged in series than through one of two vessels arranged in parallel.

The second contribution of this chapter is the construction of an improved model of the CVP, which differed in a) allowing for heterogeneous distributions of blood vessel volumes and b) expressing transit time itself as a function of time. The logistic equation was chosen as the basis of this model, given that it approximates the distribution of transit times one would expect to see in biologically realistic situations. The model's primary two parameters that govern the model are, r, indicating the deceleration of the particle, and h, the particles

capacity for reaching a certain transit time. The logistic model is also chosen because with appropriate parameter choices it excludes impossible values such as negative transit times, and allows for incorporating the effects of spatial heterogeneity into the model via its relationship to Lloyd's mean crowding index.[1, 36] Using the model given in(3.29), it is shown that when the distribution of blood vessel volumes is overdispersed, meaning there are many capillaries of very small volume compared to arteries and arterioles, the mean transit time is shorter. In some ways, this does not contradict the standard CVP, which predicts shorter transit times with more vessels running in parallel, but rather modifies it to more accurately capture the biology. More arteries and veins, which run in series, as is shown in Figure 3.1, lengthen transit time, whilst many small capillaries in series, shorten the expected transit time; the new model is thus an improvement on the CVP, rather than a rejection of it. Its ability to count for the effect of different types and arrangements of blood vessels on transit time suggests it may have promise in reconciling the results of fMRI modelling and fMRI experiments, which to date have given conflicting results.

A limitation of this chapter is that it only considers a model of the expected transit time of one oxygen particle in the absence of oxygen extraction in the brain. Oxygen extraction is required to yield an fMRI image, as the BOLD contrast converts the electrochemical difference between hemoglobin with oxygen particles attached and unattached into an image. The effect of oxygen extraction on the results given in this chapter is explored in Chapter 6. The next two chapters take the results of the this chapter and explore their implications for the design of fMRI experiments.

Chapter 4

Sequential sampling plan using a fixed level of precision

4.1 Introduction

The previous chapter introduced the concept of *mean crowding*, and the role it plays in understanding the effect of spatial heterogeneity on dynamical systems. Mean crowding, in the context of modelling the haemodynamic response, describes the relationship between the average transit time value and its variance [2, 3], where heterogeneity arises due to variability in blood vessel volumes. The experimental estimation of quantities such as the mean is more difficult in heterogeneous systems, as sampling error is considerably larger. This effect is especially noticeable when estimating the mean in an overdispersed system, where the large number of zero measurements results in a tendency to underestimate the true mean.[36] In the context of fMRI, the difficulty in relating measures of transit time to neuroimages is often attributed to difficulty in measuring transit time with precision due to the heterogeneous distribution of blood vessels throughout the brain. In the next two chapters, sampling theory is used to estimate the number of measurements that an fMRI experiment must take to estimate clinically and statistically significant variations in transit time with

acceptable precision.

Experiments in fMRI are subject to both sampling error related to heterogeneous distribution of blood vessel volumes, as described above, as well as measurement error.[37, 18] As was outlined in Chapter 2, in fMRI the BOLD signal is an image derived from the electrochemical difference in paramagnetic deoxygenated to oxygenated haemoglobin following the uncoupling principle. Measurement of the BOLD signal has an inherent level of error, like all measurement techniques.[18, 28] This error can only marginally be controlled for experimentally, but with improvements in understanding the properties of the BOLD signal, might be accounted for in analysis. Sampling error can be controlled for in experimental design by proper calculations of the sample size required to yield precise estimates. The reduction of sampling error in fMRI experiments is the focus of the next two chapters.

4.2 Methods

4.2.1 Overview

It is often claimed that the heterogeneous distribution of blood vessels in the brain is an obstacle to deriving precise estimates from fMRI experiments.[38] This need not be the case, so long as the relationship between the mean and variance in blood vessel volume is known. This chapter attempts to estimate this relationship and then begins to explore its implications for the design of fMRI experiments.

4.2.2 Data source

Experimental data from the foundational work of Grubb et al. is used to estimate the relationship between the mean and variance in blood vessel volumes.[39] This experimental study measured the transit time of chemical indicators multiple times across multiple subjects

(15 Rhesus monkeys), in order to estimate the within-host and between host variance in transit times. The indicator used in these studies was $C^{15}O$-hemoglobin tracer. This indicator was chosen because its binding to hemoglobin closely resembles the binding of oxygen, but it is not extracted in the brain like oxygen, thus yielding measurements of transit time through the brain that are unaffected by the extraction process. Most fMRI experiments use a sample size between 1 and 12 subjects, due to the high cost involved in conducting fMRI studies.[37] The experiments by Grubb et al. therefore capture the kind of variation in transit times that would be encountered in the most extensive fMRI experiments commonly used.

4.2.3 Data analysis

As described in the previous chapter, mean crowding can be expressed as a linear relationship between the mean and variance of a random variable. Experimental data can be used to estimate the parameters of the linear relationship, and then used to determine the sample size for future experiments that is adequate to estimate the mean with a specified degree of precision. Precision, D, is defined in the context of fMRI experiments as

$$D = \frac{\frac{s}{\sqrt{n}}}{\bar{t}_T}, \tag{4.1}$$

where s is the standard deviation in a sample of measurements of transit time, $s/\sqrt{n}$ is the standard error, and $\bar{t}_T$ is estimated mean transit time for a sample.[4] The minimum number of measurements of transit time, n_{min}, required to give an estimate of $\bar{t}$ with precision $\geq D$ can be given by rearranging

$$Tn \geq (a+1)/\frac{D^2 - [b-1]}{n_{min}}, \tag{4.2}$$

where T_n is the sum of transit times across n_{min} measurements, D is precision given by (4.1) and a and b are estimated from experimental data. In this case, these parameters were

estimated by fitting the model

$$t_T^* = a + b\bar{t}_T \tag{4.3}$$

to the data of Grubb et al.,[39], where t_T^* is the mean crowding of transit times. Grubb et al.'s raw data, and the estimated mean crowding t_T^* are shown in Table 4.1. In this table, n is the number of measurements per Rhesus monkey. The model was fitted using the `glm ()` command in *R*.

4.3 Results

The estimated values of a and b were -0.822 and 1.01 respectively. The model (4.3) is shown fitted to the data from Table 4.1 in Figure 4.1. The estimated values of a and b were not significantly different to the values $a = -1$, $b = 1$ that arise when (4.3) is fitted to uniformly distributed data (as described in the preceding chapter). When the estimated values of a and b and a desired level of precision, $D = .10$, were substituted into equation (4.2), it was found to result in a zero in the denominator:

$$Tn \geq (-0.822 + 1)/\frac{0.1^2 - [1.01 - 1]}{10} \tag{4.4}$$

This suggested that (4.2), developed by Kuno and Iwao [4], is not an appropriate technique for calculating the sample size that guarantees an estimate with fixed precision when measurements are uniformly distributed. This finding has not been made in the literature before. In addition, these results suggest that transit times are closer to be uniformly distributed than heterogeneously distributed, as if often claimed, if the data of Grubb et al. are taken as representative.

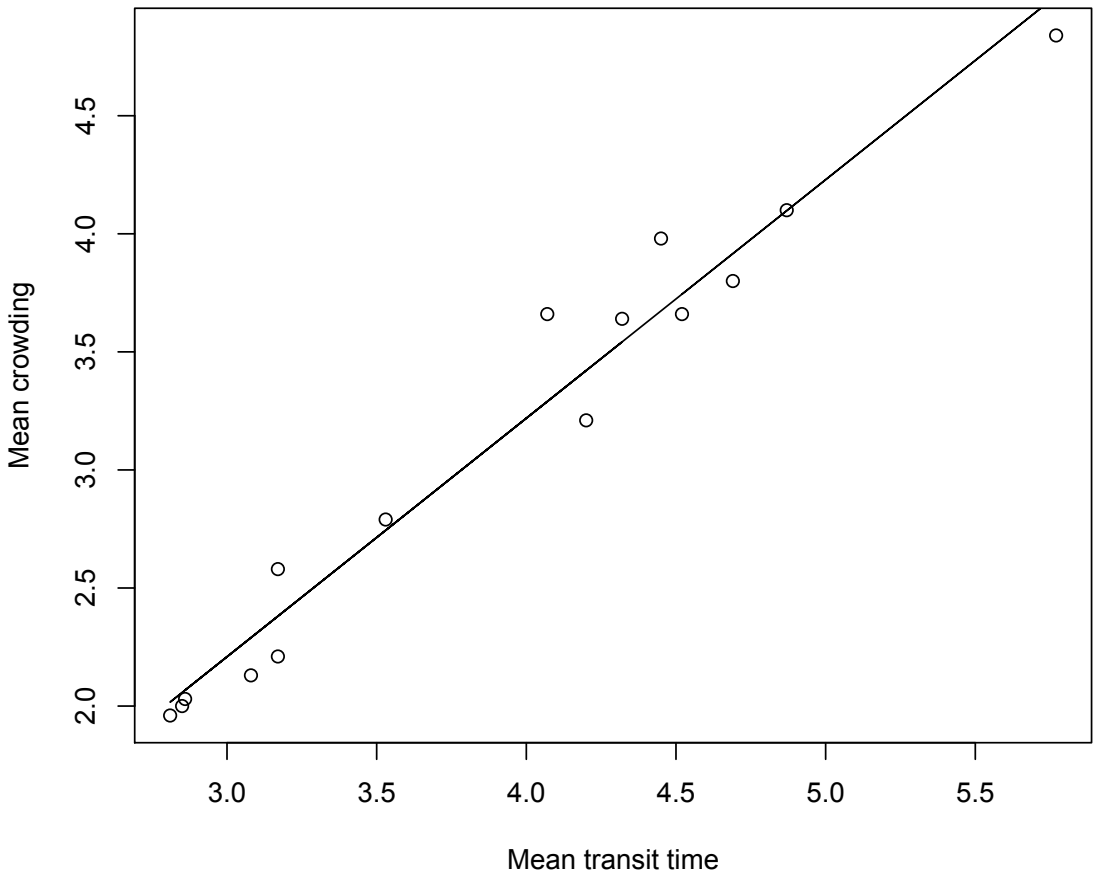

Fig. 4.1 Regression analysis for the mean crowding of transit times from Grubb et al. data.

Table 4.1 Transit times and variances for 15 rhesus monkeys

$\bar{t}$	s^2	t_T^*	n
4.2	0.06	3.21	3
3.17	0.15	2.21	3
4.32	1.38	3.64	2
4.07	2.41	3.66	3
3.53	0.90	2.79	3
3.08	0.18	2.13	2
2.86	0.50	2.03	3
3.17	1.32	2.58	3
2.81	0.43	1.96	3
2.85	0.42	2.00	2
4.45	2.38	3.98	3
4.69	0.53	3.80	4
5.77	0.44	4.84	4
4.87	1.12	4.10	3
4.52	0.60	3.66	2

4.4 Discussion

This chapter examined the requirements for fMRI experiments in two ways. First, it explored the relationship between the mean and variance of transit times by regression analysis of a foundational data set. Second, it examined the applicability of a common sample size calculation, based on the regression results, to fMRI studies. Two new contributions were made by this chapter: first, that transit times may actually be uniformly, rather than heterogeneously distributed, as is often argued. Second, results suggested that where variable measurements are uniformly distributed, it is not possible to use the relationship between mean crowding and mean density to calculate sample size. To the best of my knowledge, this result has not been previously demonstrated in the literature. This second point is primarily of theoretical interest, as in the typical applications of the mean crowding-mean density relationship (ecology and epidemiology), few outcomes or measures are uniformly distributed. Therefore,

it will not be explored further, beyond noting its relevance to future work in these fields. The finding that transit times for oxygen particles in the brain may be uniformly distributed, however, has profound implications for fMRI experiments and the clinical application of fMRI results.

As discussed in Chapter 2, it is argued that the brain accomplishes uniformity in mean transit time, arguably through a set of regulatory mechanisms. The results found in this chapter indicated the transit times were uniform [39], even though the distribution of blood vessel volumes can still be assumed to be distributed heterogeneously. This further implies the argument developed in the previous chapters that this raises problems for the correlations drawn between blood flow changes and neural activity. In turn, our focus should be redirected in equal proportion to what the effects on the BOLD signal arise from the physiological processes that maintain this uniformity in transit time.

Whilst this chapter made some important contributions, the main problem it sought to address has not been solved adequately. Therefore, the next chapter explores an alternative method for estimating the sample size with which clinically and statistically significant findings from fMRI experiments can be derived experimentally.

Chapter 5

Fixed size sampling plan

5.1 Theory and motivation for a fixed size sampling plan

The previous chapter explored whether the number of measurements required in an fMRI experiment to achieve a fixed level of precision could be estimated using the methods of Kuno and Iwao.[4] It was discovered that this calculation method was not possible where measurements were uniformly distributed, which was the case with the data set used to estimate the parameters of Iwao's mean crowding–mean relationship. This chapter tries a different approach; namely, specifying the magnitude of a clinically significant change in transit time, and estimating the sample size required to detect this change with a specified level of precision.

5.2 Methods

5.2.1 Overview

In this chapter fixed sample size plans to estimate a critical change in transit time with a minimum level of precision are evaluated using the statistical programming language *R*.

Details for the following code can be found in appendix 2. The critical change in transit time, which fMRI experiments should be able to detect, was derived from the literature; transit times > 6 seconds are commonly regarded as indicating a clinically meaningful response to a stimulus in fMRI experiments.[7]

5.2.2 Data sources

Simulated data were used to determine the sample size required to detect clinically significant variations in transit time. Fixed sample sizes of 2, 5, 10, 15, and 20 measurements (corresponding to the sample sizes commonly used in the fMRI literature) were tested for their ability to detect transit times > 6 seconds. These sample size represent the number of measurements taken in fMRI experiments, whether these comprise one measurement per subject or a set of repeated measurements from one or more subjects.

It is assumed that biologically possible transit times were between 0–15 seconds, based on values that appear in the experimental literature .[18] Transit times were taken to follow a gamma distribution with scale parameter 0.5 and shape parameter $\mu_{\bar{t}}/0.5$, where $\mu_{\bar{t}}$ is the true mean transit time. This distribution encompassed positive values between 0 and 15, with most values around 6 seconds, the theoretical "normal" transit time referred to in the literature.[18, 7] 100 samples from this distribution were drawn using Latin hypercube sampling, to ensure the whole distribution was sampled evenly. This was carried out using simulations in *R* using LHS package `lhs()`. Fixed size samples of 2, 5, 10, 15, and 20 measurements were sampled 1000 times from each of the 100 Latin hypercubes. Each instance of using a particular sample size is called a sampling iteration; thus, I simulated 1000 sampling iterations of each sample size on each of 100 simulated data sets.

5.2.3 Data analysis

The mean and variance of each 1000 sampling iterations were calculated to assess the precision of each fixed sample size at calculating transit time, where precision D is defined as

$$D = \frac{\frac{s}{\sqrt{n}}}{\bar{t}_T}, \tag{5.1}$$

s is the standard deviation of 1000 sampling iterations, $s/\sqrt{n}$ is the standard error, and $\bar{t}_T$ is estimated mean transit time for 1000 sampling iterations. The desired level of precision was the same as in chapter 4, at the level of 0.10.

In addition to calculating achieved precision, the performance of each fixed sample size was assessed by means of an operating characteristic (OC) curve. The OC gives the percentage of estimated transit times > 6 seconds, and compares these to the actual mean transit time of a given Latin hypercube. The OC function gives the probability that each sample plan will be useful in determining whether the true mean transit time exceeds the clinically significant value of 6 seconds. The OC curve was derived by fitting the estimated mean transit time for each sampling iteration to a four parameter equation using non-linear least squares. The equation is

$$\mathrm{OC} = y_0 + \frac{a}{1 + (\frac{\mu_{\bar{t}}}{\bar{t}_0})^b} \bullet \tag{5.2}$$

The lower (fixed at 0) and upper (fixed at 1) asymptotes are represented by the parameters, y_0, and, a, respectively; $\bar{t}$ is the value of $\mu_{\bar{t}_0}$ at the point of inflection. The slope parameter is b. The steepness of the curve is an indication of how close the true mean transit time, $\mu_{\bar{t}}$, is to the estimated mean transit time $\bar{t}$ for the datum. An optimum fixed size sample plan would make make as few incorrect (> 6 seconds when true transit time ≤ 6 seconds) as possible.

5.3 Results

A precision of $D \leq 0.10$ in estimate of the mean transit time was attained for all sample sizes greater that 10 over 75% of the time (see Figure 5.1). The sample sizes 2, and 5, performed less well, achieving the desired precision 40 and 50% of the time respectively. They also showed significant positive skewness in their estimates with a considerable number of outliers. The improvement in precisely estimating the mean was further evident from the change of steepness in the slopes of the OC curves, shown in Figure 5.2. In Figure 5.2, the area above the curve gives proportion of sampling iterations that estimated the mean transit time as being > 6, and the area below the curve gives the proportion of estimates of mean transit time that are ≤ 6 seconds, over 1000 sampling iterations on each data set. The x axis shows the true mean transit time for each data set. The ideal OC curve would be a step function, estimating 100% of data sets with a true mean transit time ≤ 6 as having a mean transit time ≤ 6, and zero percent of data sets with a mean transit time > 6 as having one of ≤ 6 seconds. The purple curve, showing the OC for sample size 20, shown in Figure 5.2, closely approximates the ideal step function, but others make frequent misclassification errors. For example, a sample size of 5 (red line in Figure 5.2) had an operating characteristic of 0.1 for a true mean transit time of 8 seconds. This means that the fixed sample plan of size 5 estimated the mean transit time to be ≤ 6 seconds on 10% of sampling iterations where the true mean transit time was 8 seconds.

5.4 Discussion

The results reinforce the well established difficulties with sampling in fMRI experiments. Sample sizes under 5, though commonly used experimentally, are too low to have any reliability, frequently failing to identify data sets with true mean transit times above the clinically significant threshold of 6 seconds (see Figure 5.2). This issue has been addressed extensively

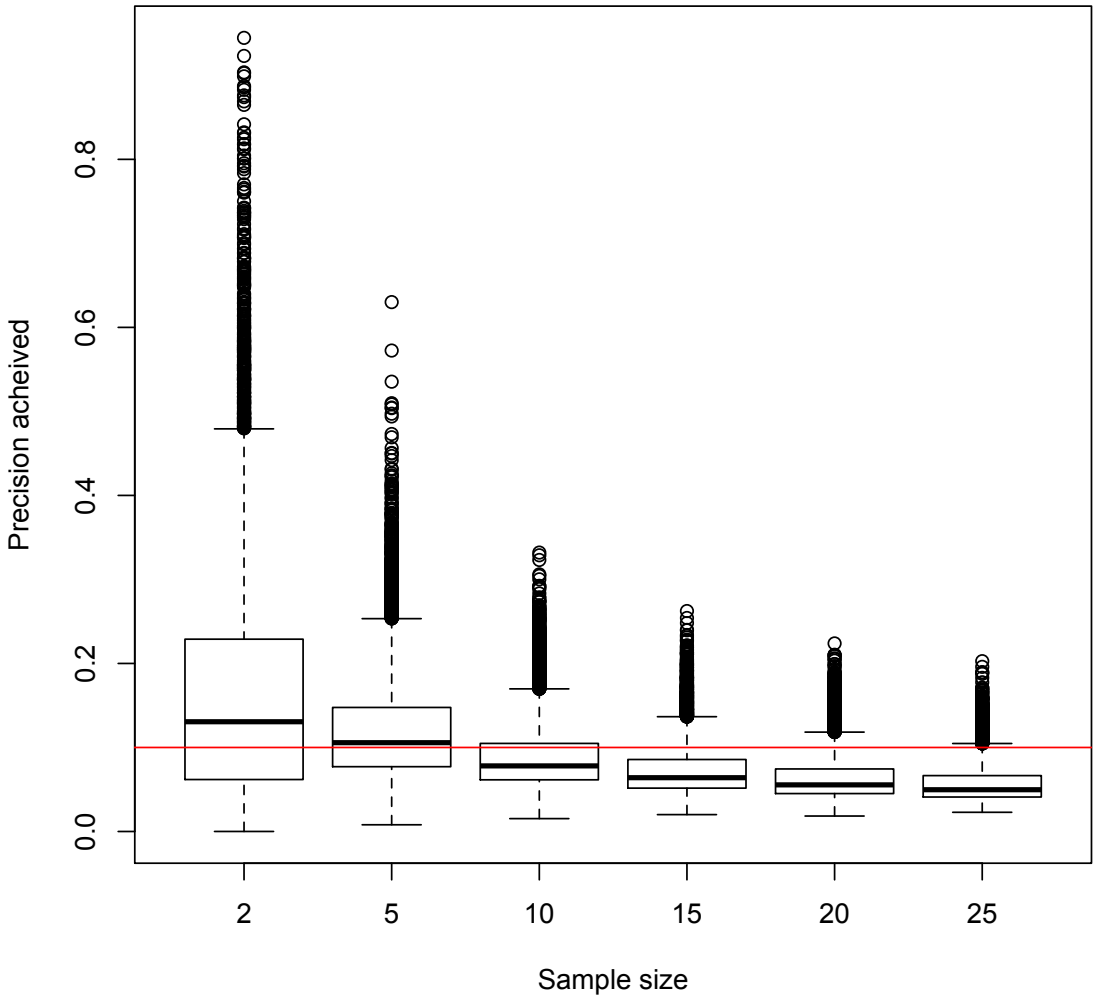

Fig. 5.1 Level of precision achieved (D = SE/$\bar{t}$) for the estimated mean transit time for 100 simulated data sets. The bottom of the boxes indicate the 25th percentile and the top of the boxes the 75th percentile; the whiskers show the 10 and 90th percentile; the dots represent any outliers. The red line indicates the target level of precision ($D = 0.10$).

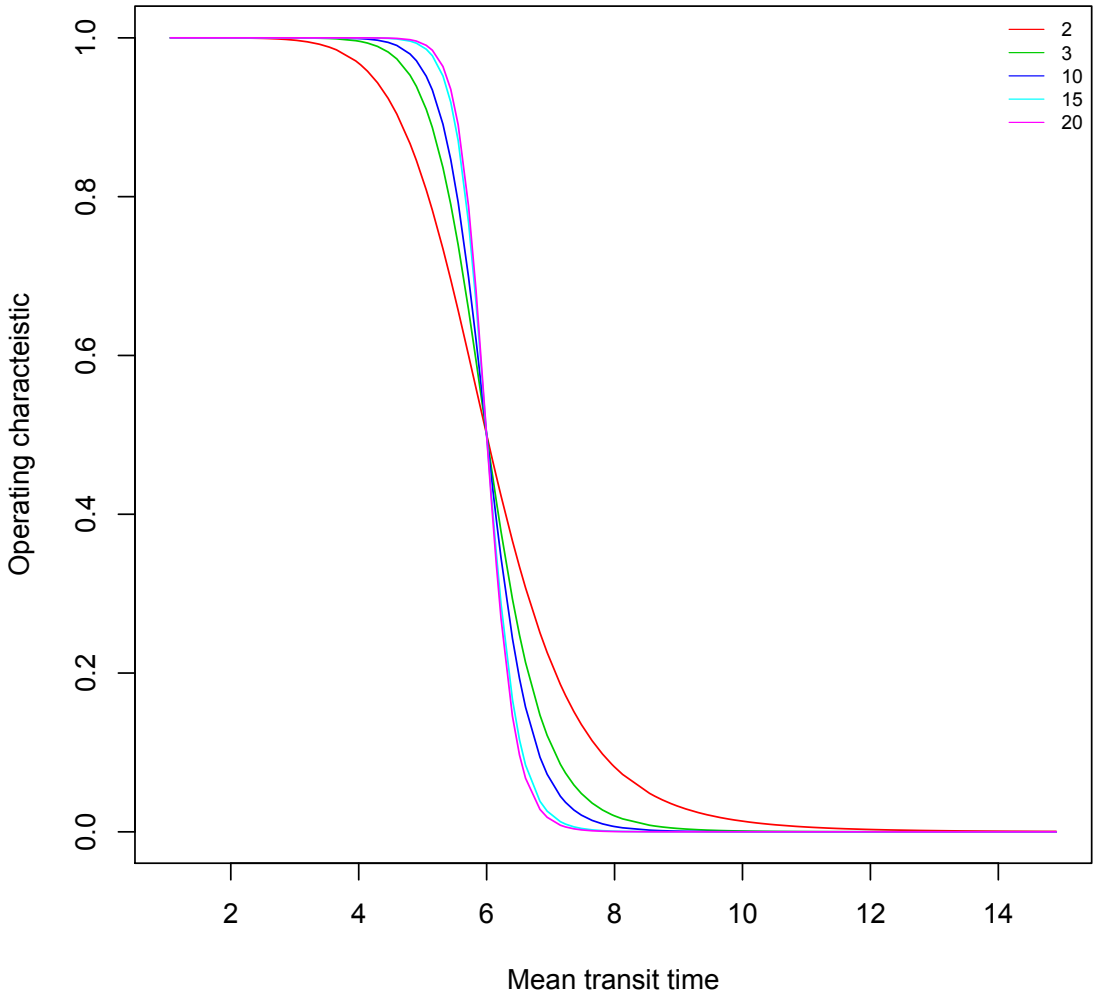

Fig. 5.2 Operating characteristic curves of the Critical value for mean transit time >6. The different colored curved lines represent fixed size samples of 2, 5, 10, 15, and 20. The steepness of each curve increases in this order as a more optimal precision is achieved. The curves were fitted using equation (5.2).

in the current literature, but without satisfactory solutions. Scholars and clinicians have called for journals to exclude papers citing sample size less than 16 .[40, 41] The limitation of this approach is twofold. First, it excludes much of the past experimental data which tends to have smaller sample sizes, but is still used in most large scale analyses today. Second, even studies with sample sizes greater than sixteen may not be reliable; meta analyses have shown significant heterogeneity between such studies arising from differences in experimental design, which reduces confidence in the results of even adequately sized studies.[42]

A limitation of the work carried out in the Chapter was the selection of only one type of theoretical distribution used for generating the simulated population to draw from: the gamma distribution. Although a reasonable choice, considering the limited information there is on population distributions of transit times, it would be an improvement to simulate fixed sampling over a larger range of different distributions. A second limit limitation of the work in this chapter is that theoretical distributions rather than empirical data were used to validate the fixed sample size plans. The reason for not using empirical data sets is related to the between-study heterogeneity discussed above. With high between study heterogeneity, it is not at all clear which empirical data sets should be used to provide an estimate of the empirical variance in transit times. In addition, there is the concern that variation in transit time measurements between studies reflects underlying bias arising from experimental techniques .[42] Therefore, our approach of specifying the extremes of transit time (0 and 15 seconds), recognising the common mean across studies of 6 seconds, and fitting an appropriate distribution to these is reasonable under the circumstances. Another approach, which we may employ in future work, would be to carry an independent meta analysis of transit times reported in empirical data, then to use a homogeneous subset of these as to parameterise a distribution for validating sampling plans. Unfortunately, this undertaking was not possible during the time constraints of this masters project.

Chapter 6

Stochastic modelling of particle transit times through capillary regions

6.1 Introduction

In the previous chapters, a logistic model describing how the transit time of a particle of oxygen through the brain differed with respect to time, blood vessel type and brain region, was developed (Chapter 3). The model was then fitted to data and the results used to examine the likely empirical distribution of transit times (Chapter 4). These results were then used to examine the question of how many experimental replicates would be required to detect a clinically significant change in transit time. The preceding chapters neglect to examine one important variable in transit time—the extraction of an oxygen particle by the brain before it fully transits through the system. The extraction process is linked to the question of clinically significant changes in transit time because there is hypothesised to be increased uptake of oxygen in situations of demand, leading to a reduction in transit times. This chapter addresses the effect of oxygen extraction on mean transit time, as predicted by the model developed in Chapter 3. This chapter is divided into two parts: part one derives formulae giving the expected effect of extraction on mean transit time. Part two uses stochastic simulation to

illustrate the effect of oxygen extraction on transit time numerically.

6.2 The expected effect of oxygen extraction on mean transit time

6.2.1 Background

The process of oxygen extraction from hemoglobin is in essence an acid base chemical reaction that occurs at the boundaries of blood vessels; understanding the effect of this process on transit time therefore has precedents in physical chemistry.[19, 43] Foundational experiments in physical chemistry by J. C. Maxwell showed that gas molecules moved faster in a smaller space, and there were more interactions between the particle and the contained, resulting in the product of more energy (heat) as a result of collisions.[44, 45] Importantly, in such a system, whilst the physical properties of gas particles, the space in which they were contained, and the heat and pressure in the space are known, the initial position and velocity of each particle is entirely random.[46] These quantities could only be considered as being described by some probability distribution. There are obvious parallels to investigating the behaviour of oxygen particles traveling in the vascular system and extracted by interactions at its boundaries. The vascular system is a confined space, transit time in smaller vessels is faster (see Chapter 3), and the initial state of the system (locations and velocities of oxygen particles) is unknown in many experiments.[22, 19] Probabilistic expressions for these quantities are now derived. First, a probabilistic representation of the model developed in Chapter 3 is developed, which permits describing the initial velocities and position of particles in the absence of prior information. Then, probabilistic expressions for the effect of extraction upon these initial transit times are developed.

6.2.2 A probabilistic model of expected transit time

The probability that a particle of oxygen to travel through a region of the brain has a particular transit time at time t, $t_T T(t)$, is $P_{t_T T}(t)$. The sum of all theoretically possible values of $P_{t_T}(t)$ is

$$\sum_{t_T(t)=0}^{\infty} P_{t_T}(t) = 1. \tag{6.1}$$

Given that the brain is composed of Q different vessel types, each with different transit times, such that

$$P_{t_T}(t) = \sum_{q=1}^{Q} p_{t_q}(t) \tag{6.2}$$

(see eqn. 3.10), it follows that the sum of all the probabilities of a particle being in region q and having a particular transit time is

$$\sum_{t_q(t)=0}^{\infty} p_{t_q}(t) = 1. \tag{6.3}$$

As described in Chapter 3, the transit time through the brain $t_T(t)$ is the sum of transit times through the respective regions, $t_q(t)$. As a particle cannot be in two regions simultaneously, $p_{t_q}(t)$ is equal to either 1 or 0. For a single oxygen particle, its expected transit time in region q at time t is therefore

$$\sum_{t_q(t)=0}^{\infty} p_{t_q}(t) t_q(t) = 0 + 1 \times \bar{t}_q(t) = \bar{t}_q(t). \tag{6.4}$$

This is in keeping with the results from the deterministic model outlined in Chapter 3.

Consider now the transit time and location of two particles $i = 1,2$ at time t. Assuming that no particle can occupy exactly the same space in region q at the same time, the transit time of any two particles cannot be the same. It follows that, if t_{qi} gives the transit time of particle i, then

$$\sum_{t_{q1}(t)=0}^{\infty} p_{t_{q1}}(t)t_{q1}(t) + \sum_{t_{q2}(t)=0}^{\infty} p_{t_{q2}}(t)t_{q2}(t) = \bar{t}_{q1}(t) + \bar{t}_{q2}(t), \tag{6.5}$$

and hence that the overall expected transit time in a two particle system is

$$\begin{aligned}\sum_{t_{q1}(t)=0}^{\infty} p_{t_{q1}}(t)t_{q1}(t) + \sum_{t_{q2}(t)=0}^{\infty} p_{t_{q2}}(t)t_{q2}(t) &= 0 + \frac{1\times\bar{t}_{q1}(t) + 1\times\bar{t}_{q2}(t)}{2} \\ &= \bar{t}_q(t).\end{aligned} \tag{6.6}$$

However, this expression does not account for which region each particle occupies. Since particle i may be in only one of $q = 1,\ldots,Q$ regions, let M define the set of values in $1,\ldots,Q$ that may contain i, and let N denote the subset of M that does not contain i. Subsequently, define the step function,

$$\sum_{q=1}^{Q} p_{t_{qi}}(t) = \begin{cases} 1 \text{ for } q \notin N \\ 0 \text{ otherwise.} \end{cases} \tag{6.7}$$

Applying (6.7) to the case of $i = 1,2$ particles in $q = 1,2$ regions, the expected transit time of particle i given that it is in region q is

$$\begin{aligned}&\sum_{t_{11}(t)=0}^{\infty} p_{t_{11}}(t)t_{11}(t) + \sum_{t_{12}(t)=0}^{\infty} p_{t_{12}}(t)t_{12}(t) + \sum_{t_{21}(t)=0}^{\infty} p_{t_{21}}(t)t_{21}(t) + \\ &\sum_{t_{22}(t)=0}^{\infty} p_{t_{22}}(t)t_{22}(t) = \frac{p_{t_{11}}\bar{t}_{11}(t) + p_{t_{12}}\bar{t}_{12}(t)}{2} + \frac{p_{t_{21}}\bar{t}_{21}(t) + p_{t_{22}}\bar{t}_{22}(t)}{2} \\ &= \bar{t}_1(t) + \bar{t}_2(t).\end{aligned} \tag{6.8}$$

It follows from (6.8) that the general form for the expected average transit time of n particles in Q regions of the brain at a time $t = 0$ in some experiment, $\bar{t}_T(t)_{(1)}$, is

$$\bar{t}_T(t)_{(1)} = \sum_{q=1}^{Q} \sum_{i=1}^{n} \left[\frac{p_{t_{qi}}(t) t_{qi}(t)}{n} \right] = \sum_{q=1}^{Q} \bar{t}_q(t). \tag{6.9}$$

Equation (6.9) constitutes the first raw moment of the distribution of particles with respect to region and transit time. The second raw moment, $\bar{t}_T(t)_{(2)}$, takes the form

$$\bar{t}_T(t)_{(2)} = \sum_{q=1}^{Q} \sum_{i=1}^{n} \left[\frac{p_{t_{qi}}(t) t_{qi}(t)}{n} \right]^2 = \sum_{q=1}^{Q} \bar{t}_q^2(t). \tag{6.10}$$

Given the binomial nature of the distribution (a particle is either in a place and has a particular transit time or not), the second central moment or variance of the distribution can be written [47],

$$\sigma_{(t)}^2 = \bar{t}_T(t)_{(2)} - [\bar{t}_T(t)_{(1)}]^2. \tag{6.11}$$

Equations (6.9) and (6.11) give the distribution of particles with different expected transit times across different regions of the brain. The effect of extraction of these oxygen particles in the capillaries upon these initial expectations will now be examined.

6.2.3 The effect of particle extraction on the probability of expected transit time

Previously, this thesis has omitted considering the effect of oxygen metabolism on transit time, but the utility of fMRI as an imaging modality, as discussed in Chapter 2, relates to its ability to detect oxygen being used by the brain. Extraction of an oxygen particle will reduce its transit time, so (6.3) needs to be modified to reflect this. Let the fraction of oxygen

particles extracted at time t be $\varepsilon(t)$, such that (6.3) is re-written as,

$$\sum_{t_q(t)=0}^{\infty} p_{t_q}(t)t_q(t)(1-\varepsilon(t)) = \bar{t_q}(t)(1-\varepsilon(t)), \tag{6.12}$$

implying the expected transit time is reduced by $\varepsilon(t)$. Specifically,

$$\sum_{t_q(t)=0}^{\infty} p_{t_q}(t)(1-\varepsilon(t)) < \sum_{t_q(t)=0}^{\infty} p_{t_q}(t). \tag{6.13}$$

The above inequality shows that taking into account extraction will reduce the transit time. Importantly, however, oxygen extraction only occurs in the capillaries, and not in other regions, with the possible exception of some small pre-capillary arterioles.[48] The amount of extraction in these arterioles is not considerable enough to be taken into consideration in this probability model, but is addressed later in the discussion of possible future work arising from this thesis. The permeability of red blood cells across the capillary wall occurs for two reasons. First, the capillaries are incredibly small in comparison to the other types of vessels. The diameter of the average capillary is similar in diameter to that of a red blood cell. The smallest capillaries tend to deform the red blood cells as they move through these small vessels.[19] As opposed to when it is in other blood vessels, it is not possible for a red blood cell to move through a capillary without making contact with cell wall, hence, increasing its chance of perfusion. Further, the capillaries do not have the smooth muscles surrounding the inner layer of endothelial cells found that is present in the arteries and arterioles, and to a lesser extent the veins and venules. This structure performs as a mechanism that allows the perfusion rate to be kept as a constant, which contributes to what is known as the auto-regulatory system.[22, 49] An example of one of these mechanisms involves a cell type in the capillaries called *pericytes*, which causes the capillaries to constrict under high levels of O^2 and to dilate under low levels of O^2, with obvious effects on extraction probability.[19] Hence, it is necessary to distinguish the overall proportion of

particles extracted at time (t), $\varepsilon(t)$, from the probability of extraction of a given particle $p_\varepsilon(t)$.

Since extraction only occurs in the capillaries, let C be the subset of values of Q where q is a capillary, so that

$$\varepsilon(t) = \begin{cases} p_\varepsilon(t) \text{ for } q \in C \\ 0 \text{ for } q \notin C. \end{cases} \tag{6.14}$$

Applying (6.14) to (6.4) gives

$$\sum_{t_q(t)=0}^{\infty} p_{t_q}(t)t_q(t)(1-\varepsilon(t)) = 0 + p_{t_c}t_c(t)(1-\varepsilon(t)) = \bar{t_c}(t)(1-p_\varepsilon(t)), \tag{6.15}$$

where c is an element of the set of capillaries C. The brain's auto regulatory mechanisms ensure that the brain will not allow the possibility of the particles to be extracted to the point of cerebral hypoxia, which would lead to loss of consciousness and ultimately death. This system allows for the conservation of oxygen particles necessary to allow the system to function properly. So, given equation (6.6) the mean transit time for the case of two particles with the extraction process is amended to become,

$$\begin{aligned} \sum_{t_{q1}(t)=0}^{\infty} p_{t_{q1}}(t)t_{q1}(t)(1-\varepsilon(t)) + \sum_{t_{q2}(t)=0}^{\infty} p_{t_{q2}}(t)t_{q2}(t)(1-\varepsilon(t)) &= \frac{\bar{t}_{c1}(t)+\bar{t}_{c2}(t)}{2}(1-\varepsilon(t)) \\ &= \bar{t}_c(t)(1-p_\varepsilon(t)). \end{aligned} \tag{6.16}$$

It follows from (6.16) the general form for the expected average transit time of n particles in Q regions of the brain at a time t, $\bar{t}_T(t)$, given (6.14) reduces to

$$\bar{t}_T(t) = \sum_{c=1}^{C}\sum_{i=1}^{n}\left[\frac{p_{t_{ci}}(t)t_{ci}(t)(1-\varepsilon(t))}{n}\right], \tag{6.17}$$

where the set of capillaries C is denoted by $c = 1,2,\ldots,C$. However, a capillary can only contain one red blood cell at a time, and the total number of particles n in the brain will be greater than the number of capillaries, C. Therefore, (6.17) further simplifies to

$$\bar{t}_B(t) = \sum_{c=1}^{C} \sum_{c=1}^{C} \left[\frac{p_{t_{cc}}(t) t_{cc}(t)(1-\varepsilon(t))}{C} \right] = \sum_{c=1}^{C} \bar{t}_c(t)(1-p_\varepsilon(t)), \tag{6.18}$$

The number of capillaries, C, is obviously very important in determining the number of extractions. The next section illustrates the effect of the number of capillaries on transit time using stochastic simulation.

6.3 Simulating particle extraction using Gillespie's algorithm

6.3.1 Overview

This section develops a stochastic simulation process to model the extraction of particles in the capillary regions. The simulation will produce an expected transit time for a particle given the capillary density in different regions. The work is based on a variant of Gillespie's stochastic simulation algorithm called the partial-propensity stochastic simulation algorithm [50]. This algorithm deals with the conditional probabilities involved by first assigning particles to their respective vessel regions, which have different number of vessels, and then determines the fate of each particle.

The algorithm reduces the computational labour needed to update the total rate of extraction by computing the parameters of the region at each new iteration. This process of incrementally updating the total rate would be very inefficient.[50] Instead, the propensities for a particle's extraction are declared globally in the code before the algorithm is run. This

does requires prior theoretical work before implementing the algorithm. From this questions can be addressed about the stochastic process of particle extraction of the expected transit times. From this foundation we can pose important questions that relate back to the previous work in other chapters: Are the transit times longer in the regions of smaller or larger capillary numbers? Is there a significant effect of extraction on transit time in regions with different capillary densities? Is there a significant difference between extracted and non extracted particle transit times? How much variation is there in the transit time for particles in different regions with different capillary numbers?

6.3.2 Implementing the algorithm

Gillespie's algorithm is an event-based algorithm, where the time period for an event to occur is first calculated, and then the event that actually occurs during the time interval is determined. Pseudocode given in Table 6.1 outlines these basic steps. R 3.4.3 for Mac OSX was used to run the simulation, and the actual code used to run the algorithm can be found in Appendix 2.

Table 6.1 Pseudocode showing the sequence of events for one iteration of the algorithm.

I	Enumerate the events $a = 1,2,\ldots,A$ that can occur during one iteration of the algorithm
II	Declare the rates of each event, and associated propensity scores
III	Determine the time interval necessary for at least one event to occur using pseudo-random number u_0
IV	Generate a second pseudo-random number u_1 to test which event occurs
V	If $u_1 <$ than the propensity for event a, event a occurs

Some fundamental biological assumptions were relied upon to implement the algorithm. First, the convention is fMRI modelling is to take the probability of extraction, $p_\varepsilon(t)$ as being constant. This is because the delivery of oxygen to the brain through the capillaries is tightly regulated. The brain is extremely susceptible to cell death (infarction), which can occur with very slight differences between supply and demand for oxygen. Clinically, the effects of infarction in the brain are seen in stroke. To avoid infarction, the central chemoreceptors of the brain regulate the flow of new, oxygenated blood to the brain, effectively meaning that the number of oxygenated red blood cells in the brain, n, is conserved. This means that the probability of extraction does not vary with supply and demand. Furthermore, the probability of extraction is regarded as fixed, because the volume of capillaries is so small (the diameter of one red blood cell) that variation in the physical characteristics of capillaries is so minute that it does not contribute meaningfully to variation in the extraction probability. This allowed the algorithm to be simplified from the standard approach described in Table 6.1. Specifically, the events that could occur at each iteration and the associated propensity scores could be treated as global constants, rather than being recalculated at each iteration.

The number of particles in the capillaries, n, and the number of capillaries were both taken to be equal to C as per (6.18). The capillaries were assigned to $r = 1, 2, \ldots, R$ regions, such that

$$n = C = \sum_{r=1}^{R} n_r, \tag{6.19}$$

with the number of oxygen particles in each region also being n_r and the rate of oxygen extraction in each region being given by

$$p_\varepsilon n_r. \tag{6.20}$$

The probability of k extractions in region r, p_{k_r} was taken to follow a Poisson distribution, such that

$$p_{k_r} = \frac{\exp^{-p_\varepsilon n_r}(p_\varepsilon n_r)^k}{k!}. \tag{6.21}$$

The events possible at each iteration of the algorithm are:

- Extraction in one of R regions; or
- No oxygen extraction.

Since the algorithm only allows for one event per iteration, the events at each iteration are mutually exclusive and independent. The probability of one extraction in *any* region is therefore governed by the rate

$$\sum_{r=1}^{R} p_\varepsilon n_r. \tag{6.22}$$

As a consequence of (6.22), the rate parameter governing the probability of no extraction in one iteration is

$$\sum_{r=1}^{R} n_r - \sum_{r=1}^{R} p_\varepsilon n_r. \tag{6.23}$$

The total rate is defined as the sum of all rates and is

$$\sum_{r=1}^{R} p_\varepsilon n_r + (\sum_{r=1}^{R} n_r - \sum_{r=1}^{R} p_\varepsilon n_r) = \sum_{r=1}^{R} n_r = n. \tag{6.24}$$

The length of one iteration, Δt, is defined as the time interval in which one event can occur (Step III in Table 6.1). This time interval is determined by the relation

$$\Delta t = \frac{-\log(u_o)}{n}, \tag{6.25}$$

where u_o is a uniformly distributed pseudorandom number. All numbers generated by *R*'s built in `runif()` function are technically pseudorandom rather than truly random, but this causes no practical difficulties in practice, as the number of possible values generated by `R` is sufficiently large as to approximate true randomness in most applications.

To determine which event occurred during interval Δt, a second pseudo-random number, u_1 was drawn and compared iteratively to the propensity scores; the propensity scores are the ratio of governing rates to total rate, (6.24). Since the extraction events are mutually exclusive, if

$$u_1 < \frac{p_\varepsilon n_r}{n}, \tag{6.26}$$

an oxygen particle was extracted in region 1; if

$$u_1 < \frac{p_\varepsilon (n_1 + n_2)}{n}, \tag{6.27}$$

an oxygen particle was extracted in region 2; and if

$$u_1 < \frac{p_\varepsilon (\sum_{r=1}^{R} n_r)}{n}, \tag{6.28}$$

an oxygen particle was extracted in region R. If

$$u_1 \geq \frac{p_\varepsilon (\sum_{r=1}^{R} n_r)}{n}, \tag{6.29}$$

no oxygen extraction events occurred in the interval Δt. It was considered that on average a particle would take $5\Delta t$ to fully pass through a capillary. Thus the algorithm outlined above was implemented 5 times for each capillary.

Results are presented for simulations using $R = 3$, where region $r = 1$ contains 10 capillaries, region $r = 2$ contains 50 capillaries, and region $r = 3$ contains 100 capillaries. The value of the extraction probability, p_ε was derived from empirical measurements suggesting that the proportion of particles extracted is 20% [16]. A value of $p_\varepsilon = 0.04$ per time step was shown to result in an overall proportion of extractions of $k/n = 0.20$ by solving (6.21) algebraically for time period $5\Delta t$. The propensity scores governing the extraction events are given in Table 6.2.

Results of the simulation were analysed using `R`. The mean transit times of extracted particles in regions 1, 2 and 3 were compared using one-way analysis of variance (ANOVA). The mean transit times of extracted versus non-extracted particles were compared using a Welch two-sample t-test. Significance was assumed at $p < 0.05$.

6.3.3 Results

There were no significant differences in mean transit time between regions. Figure 6.1 shows the distribution of transit times for extracted particles in each region. There was also no significant difference in mean transit times for extracted and non-extracted particles. Figure 6.2 shows the distribution of transit times for all extracted particles and non-extracted particles, and Figure 6.3 shows the distribution of transit times for extracted particles in each region compared to non-extracted particles.

6.4 Discussion

Neuro-imaging using the fMRI technique relies on the extraction of oxygen particles from hemoglobin producing electro-chemical changes that results in contrasting image properties

Table 6.2 Propensity scores for extraction events in $R = 3$ regions, given $p_\varepsilon = 0.04$ per time step.

Region	Number of capillaries	Extraction rate
1	10	.0025
2	50	.0125
3	100	.025

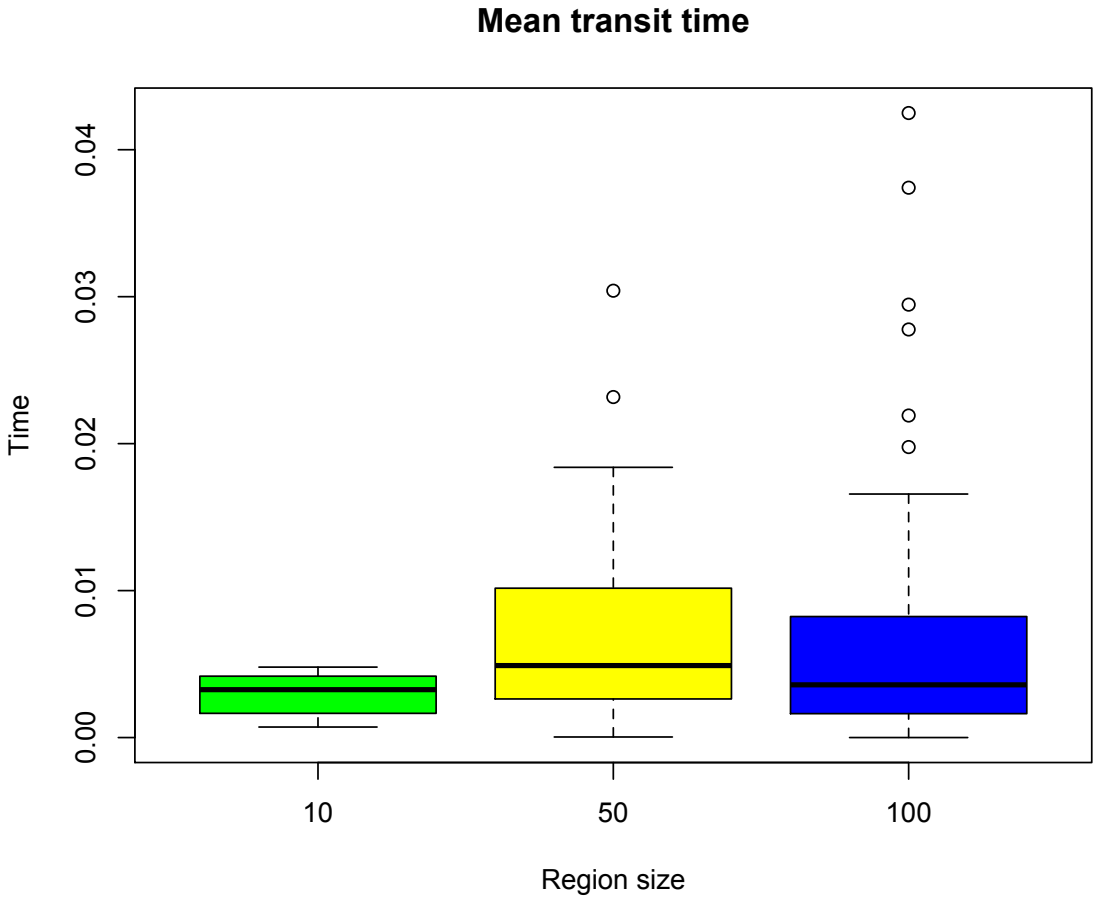

Fig. 6.1 Distribution of transit times for extracted particles in each region. The bottom of the boxes indicate the 25th percentile and the top of the boxes the 75th percentile; the whiskers show the 10 and 90th percentile. The dots above the whiskers represent the outliers.

between capillary regions with more and less extraction. If, as is argued by researchers, the extraction probability remains constant as an important part of the brain's regulatory

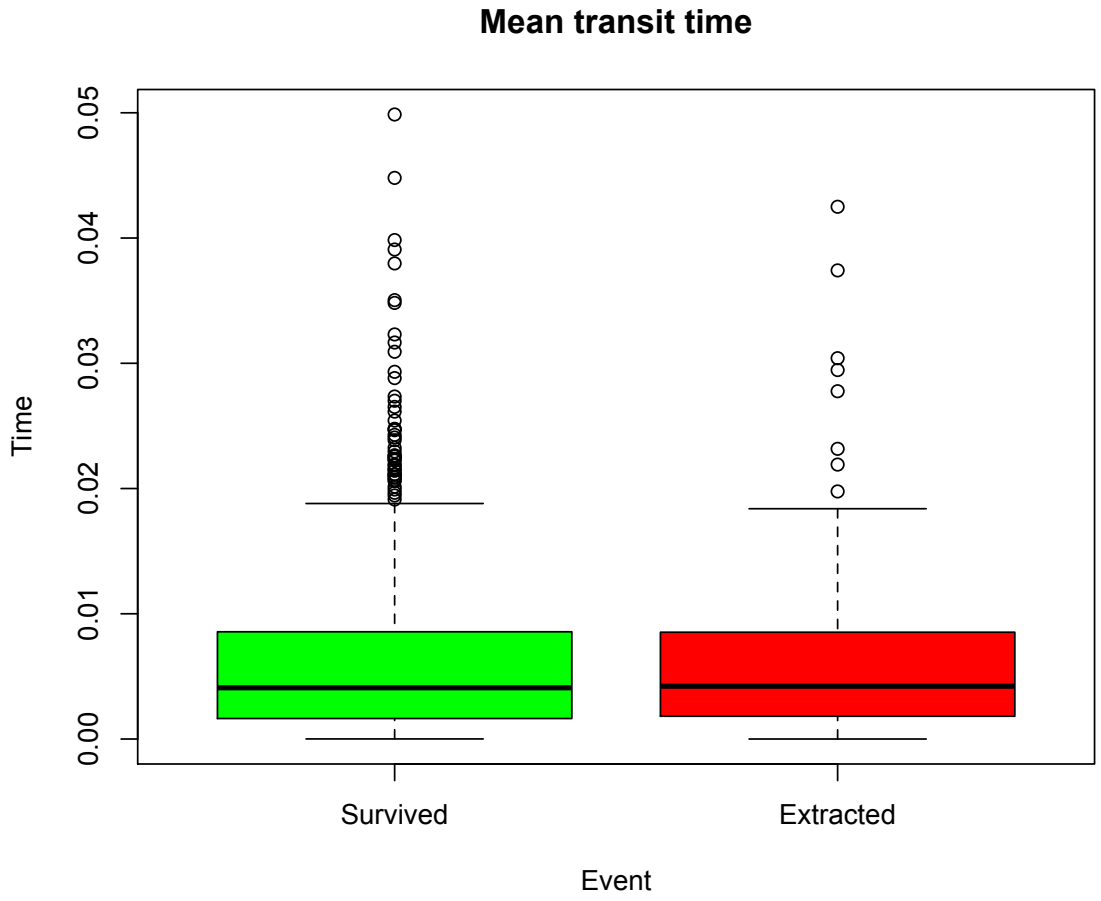

Fig. 6.2 Distribution of transit times for non-extracted (survived) particles vs. all extracted particles. The bottom of the boxes indicate the 25th percentile and the top of the boxes the 75th percentile; the whiskers show the 10 and 90th percentile. The dots above the whiskers represent the outliers.

mechanisms against hypoxia, it might be expected that the number of capillaries per region would be the most important factor in determining the relative frequency of extraction events in different regions. The calculations provided in the first part of this chapter provide an algebraic basis for this expectation, and this is reflected in the parameterisation of the stochastic simulation in the second part of this chapter. Table 6.2 shows that the propensity for extraction events is larger in regions with more capillaries. If on average the transit time through the capillary was equal to $5\Delta t$, the average time of extraction might be $2.5\Delta t$,

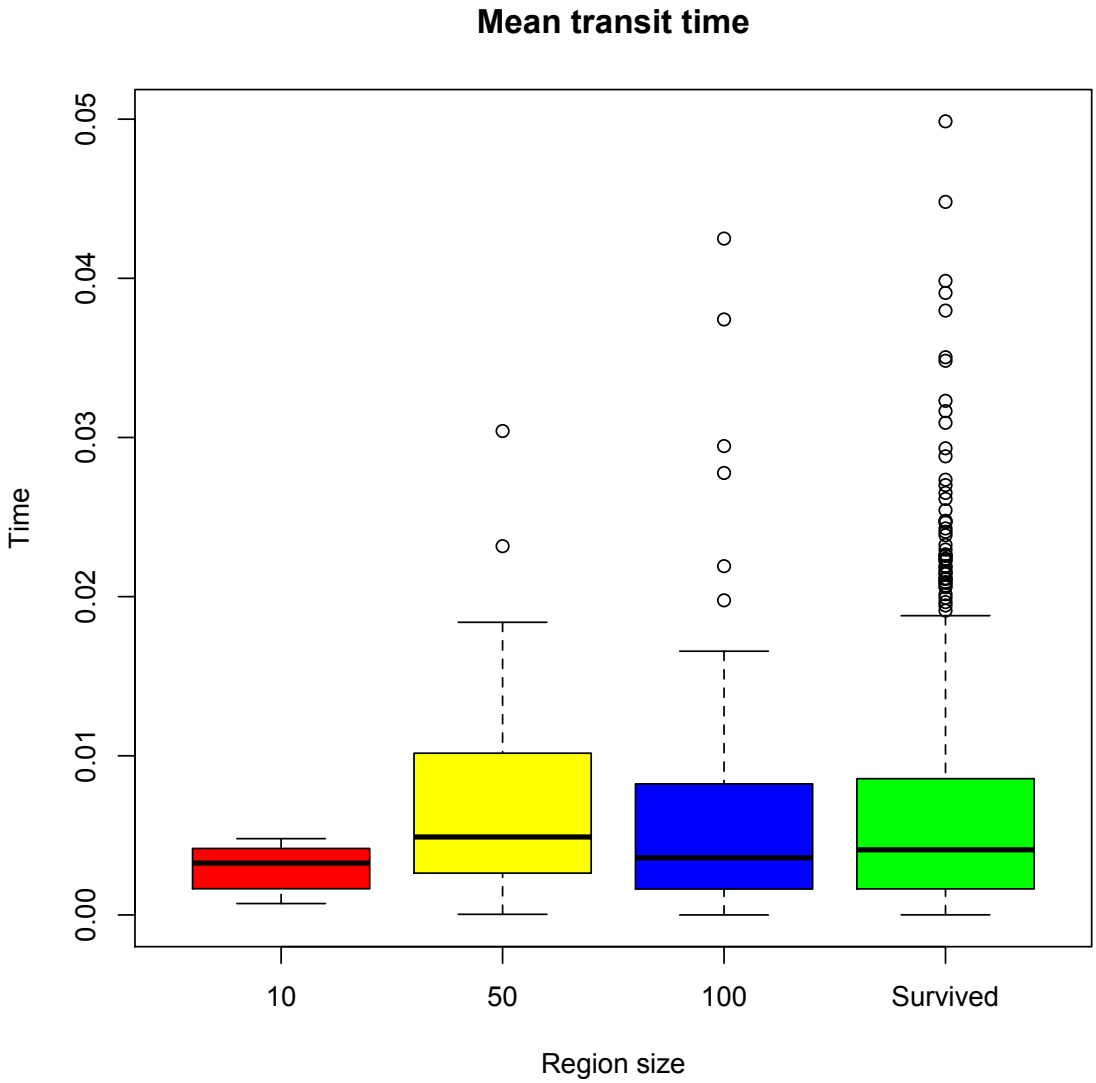

Fig. 6.3 Distribution of transit times for extracted particles in each region compared to non-extracted (survived) particles. The bottom of the boxes indicate the 25th percentile and the top of the boxes the 75th percentile; the whiskers show the 10 and 90th percentile. The dots above the whiskers represent the outliers.

suggesting that there might be significant differences in transit time between regions with greater and lesser numbers of extraction events.

Results from the simulations conducted in this chapter showed no evidence that more extractions resulted in lower transit times. This suggests that despite the heterogeneous

distribution of capillaries, the density of capillaries has little effect on mean transit time. There could be several reasons for this. The stochastic nature of the extraction process might mean that the random times at which extraction occurs results in no difference in mean transit time. On the other hand, it could be that transit times are so short in the capillaries (approaching zero seconds, according to [32]) that differences in the transit time of extracted and non-extracted particles are so small that they do not significantly effect the mean. These results suggest that detecting significant relationships between transit time and changes in fMRI images is not straightforward, and requires very large sample sizes, considering the different strata, sample sizes, and sampling methods. A detectable change in oxygenation level in the brain is not easily traced backed to a response to a stimulus, given these results. The possibility that the BOLD signal, detected by fMRI, might not be linked to increasing transit times in response to a stimulus raises important questions for the clinical and research use of fMRI. The effect of autoregulation within the brain on transit times needs to be further investigated. Canonically, the larger the BOLD signal, the more confidence a researcher might have in the stimulus being the casual factor, but this line of thinking is not supported by these results.

Chapter 7

Concluding remarks and future work

7.1 Overview

This thesis made a number of new contributions in the field of fMRI modelling research. It re-examined the phenomenon of cerebral transit time using established (differential equations) and more novel techniques (sampling techniques more commonly associated with epidemiology and ecology). A number of avenues for future work and several implications for experimental fMRI research were identified. This is pleasing considering that the scope of the work contained within this project is relatively small in scale, in contrast to diverse and large amount of growing research in the field.

There were four primary areas of focus in this thesis, each with their own unique problems, and in each of which the thesis made new contributions or proposed further areas for future research. The first area of focus was the CVP (central volume principle), which underlies many important fMRI models. Findings related to this area of focus are included in Chapters 3 and 6 of the thesis. The second area of focus was applying my findings regarding the CVP to evaluating the sample sizes required for reliable fMRI experimental studies. This area of focus is examined in Chapters 4 and 5. The final area of focus was exploring the effects that

extraction of oxygen particles in the brain might have on the results presented in previous chapters. This work is included in Chapter 6. Contributions made by each Chapter in these areas are now described.

7.2 Contributions of each chapter

Chapter 3 made two new contributions relating to the CVP. The first contribution of Chapter 3 was demonstrating that the traditional form of the CVP, given in equation (2.1) does not account for different spatial distributions of different types of blood vessels. The CVP was first developed experimentally from ground breaking research in physiology and fluid dynamics dating back to over 100 years, but which dealt with the pulmonary and systemic, rather than cerebral, circulation.[31, 32] Today, it is understood that the intricate and complicated structure of the cerebral cardiovascular system is quite different to that of the systemic and pulmonary circulations. For example, a relatively larger proportion of the cerebral circulation is comprised of small-volume capillaries, which will make a correspondingly small contribution to transit time compared to the larger diameter arteries and veins that comprise a smaller part of the cerebral circulation. Therefore, the cerebral circulation is comprised of a spatially heterogeneous distribution of blood vessel types. It follows that the canonical CVP will not accurately model transit time in the cerebral circulation. Chapter 3 also showed that, importantly, spatial heterogeneity of blood vessels will also result in temporal heterogeneity in transit times for a given oxygen particle. If a particle moves through different vessel types with different volumes, it will have a different transit time in each (short in the small volume capillaries, and long in the large volume arteries). These findings led to the next contribution of the chapter.

The second novel contribution of Chapter 3 was developing a variant of the CVP that accounts for the effect of spatially and temporally heterogeneous blood vessel volumes on

transit time. This model was based on that of Waters et al.[1], and incorporated a linear form of the mean crowding–mean density relationship into the logistic differential equation to account for the effect of spatial heterogeneity. This model is given in equation (3.15). The idea of using a differential equation to express transit time as a function of time arose from the temporal heterogeneity noted above. The model was based on the assumption that as a particle changed location spatially with respect to time, the change in its expected transit time with respect to the environment (blood vessel volume) at each moment could be expressed by a derivative. Using this model, it was straightforward to demonstrate the effect of a heterogeneous distribution of blood vessels on mean transit time, as shown in equation (3.20). For example, in overdispersed systems with more small-volume vessels (such as brain, which has a preponderance of capillaries), the mean transit time was smaller. Whilst the effect of spatial heterogeneity on dynamical systems, and the use of mean crowding to account for these effects, is common in epidemiology and ecology [1, 51, 36], it has not previously been employed in fMRI modelling.

In summary, after identifying problems with the application of the traditional CVP to modelling cerebral oxygen transport, Chapter 3 developed a new model for oxygen particle transit time in the brain that appeared to be more realistic, thus making several new contributions to fMRI research. Two possible limitations of the research conducted in Chapter 3 can be identified. First, the focus of the model was macroscopic differences in blood vessel volumes, in the sense that it was captured spatial heterogeneity between vessel types, but not within them. Arguably, microscopic variation in some vessel types (particularly the capillaries) might be more important than macroscopic variation in determining clinically significant variations in transit time. The model could be further improved to address this possibility by incorporating both microscopic and macroscopic variability in blood vessel volumes. On the other hand, a key strength of my model is that it lacks the complexity of some other

models involving partial differential equations.[28, 35] For that reason, mine might be more accessible to clinicians interested in fMRI, and this limitation might be a strength in some respects. Second, the model, which is deterministic, did not examine what effect the stochastic process of oxygen extraction in the capillaries might have on its predictions of transit time. This issue was, however, examined in Chapter 6 using stochastic modelling. The conclusions drawn in Chapter 6 are discussed in more detail below, but it is worth noting here that oxygen extraction had no significant effect on mean transit time. Therefore, not considering the effect of oxygen extraction on transit time in this chapter is not a very important limitation.

The difficulties that spatial heterogeneity poses for sample size estimation and experimental design are well recognised in disciplines such as ecology.[52] Chapters 4 and 5 explored the adequacy of sample sizes in fMRI commonly used in fMRI experiments using methods developed in ecology and epidemiology.[53, 52] Chapter 4 developed an enumerative sampling plan based on the mean crowding–mean density relationship to determine the number of measurements required to estimate mean transit times with a pre-determined level of precision. Empirical data from Grubb et al.[39] were used to parameterise the mean crowding–mean density relationship. It was expected, from the literature reviewed in Chapter 2 and Chapter 3 that the parameters best fitting the mean crowding–mean density relationship to the Grubb data would indicate overdispersion. Surprisingly, given the heterogeneous distribution of blood vessels in the brain, the parameters that maximised the fit of the model to the data indicated that transit times were uniformly distributed (see Figure 4.1). This result has obvious implications for fMRI research. The foundational experimental study by Grubb et al. contains one of the largest sets of measurements included in the neuroimaging literature, and is one of few that specifically aims to estimate transit time. The fact that its data are uniformly distributed has not, to the best of my knowledge, been previously remarked upon in the literature. This finding contradicts common claims about fMRI research (i.e. that

transit times are inherently variable), and it is notable that many of the studies reporting heterogeneity in transit times use much smaller sample sizes than Grubb et al., and estimate transit time as a quantity that is autocorrelated with BOLD signalling, and hence important for image processing, rather than as an outcome measure in its own right. The results of Chapter 4 give reason to re-examine assertions about the heterogeneity of cerebral transit times commonly made in the literature. Chapter 4 also made another novel contribution as a side result. It showed that enumerative sampling plans on the mean crowding–mean density relationship are mathematically intractable for uniformly distributed variables see equation (4.4). To the best of my knowledge, this is the first time that this result has been shown in the literature. Whilst is has limited utility in fMRI research, it will have implications for fields where this sampling methodology is commonly used, such as ecology.[52]

The inappropriateness of the enumerative sampling plan methodology investigated in Chapter 4 for uniformly distributed data required exploring a different approach to examine the effect of transit time distributions on required sample size for fMRI experiments. Chapter 5 was developed in response. This chapter validated the performance of fixed sample sizes at detecting clinically significant changes in transit time using simulated, rather than empirical, data. The simulated data were, however, based on empirically derived parameters, and the fixed sample sizes evaluated corresponded to the sample sizes commonly employed in fMRI experiments. Most experimental designs in fMRI experiments are based on the assumption that the primary cause of detectable changes in the BOLD contrast arise from neural activation in response to a stimulus. This clinically significant change in the BOLD, theoretically, might also be reflected in clinically significant increases in transit time. Therefore, the fixed sample size plans were evaluated for their ability to detect clinically significant increases in mean transit time (> 6 seconds) with an acceptable level of precision (0.10). None but the largest sample sizes tested could accurately identify an increase in mean transit time, and a

considerable number of outliers (extreme value estimates) generated using all the sample sizes of interest. The results shown in this chapter reinforce the considerable concern in the fMRI field that the sample sizes commonly used in the field give unacceptable numbers of false positive results.[1] The results in this chapter show that a minimum sample size of 16 in fMRI studies, as recommended by most clinicians[40], would be better than 5 or 10, and would achieve the required precision of 0.10 most of the time (see Figure 5.1). On the other hand, even sample sizes of 20 still made a substantial number of mis-classifications (see figure 5.2). Therefore, while the results in this chapter support some of the criticisms previously made of experimental designs in fMRI research, they also suggest that measures recommended to improve the quality of experimental studies do not go far enough.

The work preceding Chapter 6 developed a deterministic model that could describe how the mean transit time of oxygen particles in the brain changed with blood vessel type, spatial area, and changes over time, but neglected to introduce particle extraction into the analysis. Furthermore, the effect of microscopic and stochastic variability on the predictions of the model were neglected. Chapter 6 develops a stochastic model that incorporates these effects and demonstrates their expected impact on transit time numerically. This chapter was divided into two parts. The first part initially incorporated the effects of stochasticity into the logistic model developed in Chapter 3, and then extended this to include the effect of particle extraction probability on the mean transit time of a particle. The second part of the chapter used stochastic simulation to illustrate the effect that oxygen extraction, which only occurs in the capillaries, has on transit time. The results produced showed no significant changes in transit times between regions with more capillaries to those with less. This finding supported the unexpected finding in Chapter 4 than an empirical data set of transit times was uniformly distributed. If factors such as oxygen extraction and heterogeneous distributions

[1] False positive results are those where a clinically significant change in mean transit time is detected, but in fact has not occurred.

of blood vessel volumes have little effect on transit time, variability in transit time cannot be the main factor causing difficulties in drawing reliable inferences from fMRI experiments. As shown in Chapter 5, sample sizes in many experiments continue to be inadequate for drawing reliable inferences, even where there is little heterogeneity in transit times. The main contribution of this thesis may well lie in posing questions about the assumption of gross variability in transit times as a source of error in fMRI experiments. This finding, in turn, leads to a number of avenues for future research relating not to the sources of variability in fMRI, but why such an anatomically heterogeneous system as the cerebral circulation should yield homogeneous transit times and constant probabilities of oxygen extraction.

7.3 Future work

The results in Chapters 3 to 6 suggested many opportunities for future research. The main avenues of future research will relate to reconciling the conflicting findings of this thesis. According to the mathematical model presented in Chapter 3, the CVP does not accurately predict transit time in a system with many small vessels. If the capillaries, for example, were to be distributed in higher numbers than other vessel types should produce a shorter expected transit time. This expectation was not reflected in results presented in Chapter 6, where mean transit time did not vary between systems with different numbers of capillaries. Similarly, analysis of a foundational data set in Chapter 4 suggested a uniform distribution of transit times. Mathematics and physiology both suggest some possible explanation for these conflicting findings. More than a century ago, Stewart postulated that given that the volume of capillaries is infinitesimally small, the transit time through the capillaries must be close to zero.[32] This observation suggests a mathematical explanation. If the differences in volume between capillaries are themselves infinitesimally small, this suggests that measuring meaningful differences in mean transit time between different regions might be almost impossible with current technology. Research in physiology suggests another explanation for these

findings. Given that the brain is particularly susceptible to damage from ischaemia (lack of blood flow), it possesses sophisticated mechanisms (such as the central chemoreceptors) for regulating blood flow. It is easy to see how the demand for constant blood supply might lead to uniformity in transit times, functional processes that regulate uniform flow times to account for any spatial heterogeneity. This lead me to conclude that if the results of this research project are correct and there is uniformity in transit time, this must be arise from either the brain's physiological regulation of blood flow, infinitesimally small differences in transit times beyond the measurement capabilities of current tools, or a combination of both. This hypothesis will need careful investigation by future researchers in light of the results presented in this thesis. In general, however, this finding supports the conclusions of other researchers that much more needs to be understood at a microscopic level about the behaviour of the systems that regulate blood flow to the brain before the results of mathematical models and experimental fMRI studies will be able to be reconciled.

Despite the fact that some results in this thesis contradicted frequently employed assumptions in fMRI research about the heterogeneity of transit times, the thesis nonetheless has important implications for interpreting experimental studies that employ these assumptions. The results presented in Chapter 5 showed that the vast number of sample sizes employed in fMRI experiments are inadequate for detecting changes in transit time that have been deemed to be clinically significant. Admittedly, the evaluation presented in Chapter 5 had the important limitation of relying on simulated data to evaluate the sampling plans. Unfortunately, due to the small sample sizes uses in many empirical studies, the performance of the sampling plans was unable to be evaluated using empirical data sets. This is not a limitation unique to this thesis, but to attempts to develop and validate new experimental protocols in the fMRI field as whole. Part of this is because the observable measurements of transit times are not in the orders of magnitude similar to phenomena studies in ecology and

epidemiology, and may in fact be infinitesimal, as noted above. There are concerted efforts to improve this aspect of the field with suggestions of minimum sample sizes and the use of meta-analysis, but even with the latter approach, it will be some time before enough large size studies are available to limit type I and II errors in meta-analyses.[54] The implications of the results presented in Chapter 5 for sample size selection in experimental fMRI studies could be meaningful in future research.

A further direction for future work is improving the algorithm presented in Chapter 6. Possible improvements that would make the algorithm more realistic would be allowing for multiple events (such as the extraction of multiple particles in multiple blood vessels) to occur at each time step. This would, however, require a new approach than Gillespie's algorithm, which is fundamentally based on calculating the propensity for single events, then occurring which event (non events) occur in a given time step. Exploring agent based modelling frameworks to simulate oxygen transport and extraction in the brain could be a useful avenue of future research in developing more realistic stochastic simulations than the one developed in Chapter 6.

7.4 Conclusion

This thesis used several approaches, both mathematical and statistical, to address known issues in fMRI modelling. I drew from applications studies outside of fMRI in developing my methods, hoping that the use of novel methods might yield novel results. Alternatively, at least I would show that novel methods produced similar results to what has already been reported in the literature. In the end, I believe that this thesis did make several new contributions to knowledge, as summarised above.

The most important of these contributions was, in my opinion, highlighting the importance of the auto-regulation process in the brain as a possible mechanism for ensuring homogeneous blood flow and transit times. Whilst infinitesimally small differences in transit times may present an alternative explanation for the results presented in this thesis, I believe that further collaboration between physiologists and modellers is a better avenue for future research. It is always possible to improve measurement tools, but if the brain is fundamentally governed to ensure uniform blood flow and transit times, improving experimental measurements will not help—a precise measurement is not going to detect something when there is nothing to measure. While Chapter 5 makes important contributions regarding calculating sample size for fMRI research carried out in the current paradigm, the results shown in Chapters 4 and 6 suggest the need for paradigm change. Despite the vast literature exploring the nature of blood flow dynamics,[29, 31, 32, 25, 24] there is nothing close to any sort of consensus on how blood flow responds to stimuli. In response to this confusion, fMRI research characteristically treats cerebral blood flow as being a "black box" where a single input (an oxygen particle) is linked to a single output (extraction of the oxygen particle or not), but anatomical and physiological processes in between are ignored because they are poorly understood. This scientific approach is only tenable up until the point where it begins to be contradicted by further experimental evidence. The historical trend in most scientific research fields is to undergo a series of paradigm shifts regarding the fundamental principles of the objects of study and the appropriate methods for interpreting meaningful results.[55] When a science is in its infancy, which neuroimaging is, models need to draw on assumptions (often from other disciplines), which may or may not be realistic. Over time, however, experimental evidence arises that indicates that these assumptions and models need to be reevaluated. The CVP, foundational to the models of the BOLD contrast and fMRI, was shown in Chapter 3 of this thesis to be unrealistic. A reliable understanding and measurement of transit time is vital to determining what produces the BOLD signal, an essential feature

undergirding the experimental design in all fMRI studies. Despite developing an improved model for transit time in Chapter 3, results presented in Chapters 4 and 6 suggest that the importance of the improved model will depend on resolving the fundamental physiological issue of just how much variability there is in transit time, given the brain's sophisticated auto-regulatory mechanisms. It was a focus of this thesis to both evaluate the quality of current practices and assumptions in fMRI research, and to provide new models and tools to improve the work carried out in the field. The results contained in Chapters 3 to 6 present numerous avenues for future research in furthering these goals.

7.5 Summary

In summary, this thesis used the mean crowding–mean density relationship to show the theoretical underpinnings of many fMRI models are unrealistic, and in particular to illustrate how the unrealistic assumptions of the CVP may influence the results of modelling studies. Chapter 5 then showed how, irrespective of the spatial distribution of blood vessels, most fMRI experiments employ sample sizes too low to make reliable inferences. Finally, Chapters 4 and 6 suggested far more homogeneity in transit times than expected by employing the assumptions typically used by fMRI modellers. This suggested the need for more physiological research exploring the regulation of oxygen transit time in the brain, in order to make findings from fMRI experiments more relevant to clinical practice.

References

[1] Waters EK, Sidhu HS, Sidhu LA, Mercer GN. Extended Lotka–Volterra equations incorporating population heterogeneity: Derivation and analysis of the predator–prey case. Ecological Modelling. 2015;297:187–195.

[2] Iwao S. A new regression method for analyzing the aggregation pattern of animal populations. Researches on Population Ecology. 1968;10(1):1–20.

[3] Lloyd M. Mean Crowding. The Journal of Animal Ecology. 1967;p. 1–30.

[4] Kuno E. A new method of sequential sampling to obtain the population estimates with a fixed level of precision. Researches on Population Ecology. 1969;11(2):127–136.

[5] Bullmore E. The future of functional MRI in clinical medicine. Neuroimage. 2012;62(2):1267–1271.

[6] Poldrack RA. The future of fMRI in cognitive neuroscience. Neuroimage. 2012;62(2):1216–1220.

[7] Lindquist MA. The statistical analysis of fMRI data. Statistical Science. 2008;p. 439–464.

[8] Uttal WR. Mind and brain: A critical appraisal of cognitive neuroscience. Mit Press; 2011.

[9] Uttal WR. Reliability in cognitive neuroscience: A meta-meta-analysis. MIT Press; 2013.

[10] McCabe DP, Castel AD. Seeing is believing: The effect of brain images on judgments of scientific reasoning. Cognition. 2008;107(1):343–352.

[11] Wager TD, Lindquist MA. Principles of fMRI. Leanpub. Available from http://refhub.elsevier.com/S1053-8119(17)30324-5/sbref24 or directly at https://leanpub.com/principlesoffmri; 2015.

[12] Wardlaw JM, O'Connell G, Shuler K, DeWilde J, Haley J, Escobar O, et al. "Can it read my mind?"–What do the public and experts think of the current (mis) uses of neuroimaging? PloS one. 2011;6(10):e25829.

[13] Racine E, Bar-Ilan O, Illes J. fMRI in the public eye. Nature Reviews Neuroscience. 2005;6(2):159.

[14] Gazzaniga MS. The cognitive neurosciences. MIT press; 2004.

[15] Poldrack RA. Can cognitive processes be inferred from neuroimaging data? Trends in cognitive sciences. 2006;10(2):59–63.

[16] Buxton RB, Frank LR. A model for the coupling between cerebral blood flow and oxygen metabolism during neural stimulation. Journal of Cerebral Blood Flow & Metabolism. 1997;17(1):64–72.

[17] Rasmussen PM, Jespersen SN, Østergaard L. The effects of transit time heterogeneity on brain oxygenation during rest and functional activation. Journal of Cerebral Blood Flow & Metabolism. 2015;35(3):432–442.

[18] Handwerker DA, Gonzalez-Castillo J, D'esposito M, Bandettini PA. The continuing challenge of understanding and modeling hemodynamic variation in fMRI. Neuroimage. 2012;62(2):1017–1023.

[19] Huettel SA, Song AW, McCarthy G. Functional magnetic resonance imaging. vol. 1. Sinauer Associates Sunderland; 2004.

[20] Logothetis NK. What we can do and what we cannot do with fMRI. Nature. 2008;453(7197):869–878.

[21] Dawson MJ. Paul Lauterbur and the Invention of MRI. MIT Press; 2013.

[22] Jespersen SN, Østergaard L. The roles of cerebral blood flow, capillary transit time heterogeneity, and oxygen tension in brain oxygenation and metabolism. Journal of cerebral blood flow & metabolism. 2012;32(2):264–277.

[23] Rosen BR, Savoy RL. fMRI at 20: has it changed the world? Neuroimage. 2012;62(2):1316–1324.

[24] Buxton RB. Dynamic models of BOLD contrast. Neuroimage. 2012;62(2):953–961.

[25] Klingensmith III WC. The Mathematics and Biology of the Biodistribution of Radiopharmaceuticals-A Clinical Perspective. Springer; 2016.

[26] Buxton RB, Uludağ K, Dubowitz DJ, Liu TT. Modeling the hemodynamic response to brain activation. Neuroimage. 2004;23:S220–S233.

[27] Fox PT, Raichle ME. Focal physiological uncoupling of cerebral blood flow and oxidative metabolism during somatosensory stimulation in human subjects. Proceedings of the National Academy of Sciences. 1986;83(4):1140–1144.

[28] Buxton RB. Introduction to functional magnetic resonance imaging: principles and techniques. Cambridge university press; 2009.

[29] Zierler KL. Theoretical basis of indicator-dilution methods for measuring flow and volume. Circulation Research. 1962;10(3):393–407.

[30] Cipolla MJ. The cerebral circulation. Integrated systems physiology: From molecule to function. 2009;1(1):1–59.

[31] Zierler K. Indicator dilution methods for measuring blood flow, volume, and other properties of biological systems: a brief history and memoir. Annals of biomedical engineering. 2000;28(8):836–848.

[32] Stewart G. Researches on the circulation time in organs and on the influences which affect it. The Journal of physiology. 1893;15(1-2):1–89.

[33] Zierler KL. Equations for measuring blood flow by external monitoring of radioisotopes. Circulation research. 1965;16(4):309–321.

[34] Brogioli D, Vailati A. Diffusive mass transfer by nonequilibrium fluctuations: Fick's law revisited. Phys Rev E. 2000 Dec;63:012105. Available from: https://link.aps.org/doi/10.1103/PhysRevE.63.012105.

[35] Zheng Y, Johnston D, Berwick J, Chen D, Billings S, Mayhew J. A three-compartment model of the hemodynamic response and oxygen delivery to brain. Neuroimage. 2005;28(4):925–939.

[36] Kuno E. Aggregation pattern of individuals and the outcomes of competition within and between species: differential equation models. Researches on Population Ecology. 1988;30(1):69–82.

[37] Poline JB, Breeze JL, Ghosh S, Gorgolewski K, Halchenko YO, Hanke M, et al. Data sharing in neuroimaging research. Frontiers in neuroinformatics. 2012;6.

[38] Birn RM. The role of physiological noise in resting-state functional connectivity. Neuroimage. 2012;62(2):864–870.

[39] Grubb RL, Raichle ME, Eichling JO, Ter-Pogossian MM. The effects of changes in PaCO2 cerebral blood volume, blood flow, and vascular mean transit time. Stroke. 1974;5(5):630–639.

[40] Friston K. Ten ironic rules for non-statistical reviewers. Neuroimage. 2012;61(4):1300–1310.

[41] Lindquist MA, Caffo B, Crainiceanu C. Ironing out the statistical wrinkles in "ten ironic rules". Neuroimage. 2013;81:499–502.

[42] Shohamy D, Myers C, Grossman S, Sage J, Gluck M, Poldrack R. Cortico-striatal contributions to feedback-based learning: Converging data from neuroimaging and neuropsychology. Brain. 2004;127(4):851–859.

[43] Maxwell JC. A treatise on electricity and magnetism. vol. 1. Clarendon press; 1881.

[44] Maxwell JC, Pesic P. Theory of heat. Courier Corporation; 2001.

[45] Maxwell JC, et al. IV. On the dynamical theory of gases. Philosophical transactions of the Royal Society of London. 1867;157:49–88.

[46] Maxwell JC, et al. II. On the dynamical theory of gases. Proceedings of the Royal Society of London. 1867;15:167–171.

[47] Iwao S. A note on the related concepts ‘mean crowding’and ‘mean concentration’. Researches on Population Ecology. 1976;17(2):240–242.

[48] Krieger SN, Streicher MN, Trampel R, Turner R. Cerebral blood volume changes during brain activation. Journal of Cerebral Blood Flow & Metabolism. 2012;32(8):1618–1631.

[49] Villringer A, Them A, Lindauer U, Einhäupl K, Dirnagl U. Capillary perfusion of the rat brain cortex. An in vivo confocal microscopy study. Circulation research. 1994;75(1):55–62.

[50] Komarov I, D’Souza RM. Accelerating the gillespie exact stochastic simulation algorithm using hybrid parallel execution on graphics processing units. PLoS One. 2012;7(11):e46693.

[51] Hagihara A. The time sequence of the relation between mean crowding and mean density with some population processes. Researches on population ecology. 1976;17(2):224–239.

[52] Waters EK, Furlong MJ, Benke KK, Grove JR, Hamilton AJ. Iwao’s patchiness regression through the origin: biological importance and efficiency of sampling applications. Population ecology. 2014;56(2):393–399.

[53] Waters EK, Hamilton AJ, Smith AM, Philp DJ, Donovan B, Regan DG. Fixed sized samples for type-specific surveillance of human papillomavirus in genital warts. Sexual health. 2013;10(1):95–96.

[54] Turner RM, Bird SM, Higgins JPT. The Impact of Study Size on Meta-analyses: Examination of Underpowered Studies in Cochrane Reviews. PLOS ONE. 2013 03;8(3):1–8. Available from: https://doi.org/10.1371/journal.pone.0059202.

[55] Kuhn TS. The structure of scientific revolutions. University of Chicago press; 2012.

Appendix A

Appendix 1: Glossary

Abbreviation	Definition
Asl(fMRI)	Arterial spin labeling fMRI
CAT	Computed axial tomography
CBV	Cerebral Blood Volume
BOLD	Blood Oxygenation Level Dependant
$CMRO_2$	Cerebral Metabolic Rate Oxygenation
CVP	Central Volume Principle
fMRI	functional Magnetic Resonance Imaging
HRF	Haemodynamic Response Function
IDP	Indicator Dilution Principle
MRI	Magnetic Resonance Imaging
OEF	Oxygen Extraction Fraction
PET	Positron Emission Tomography
ROI	Region of Interest
F	Blood flow
$\bar{t}$	Mean transit time
$\bar{t_q}$	Mean transit through any vessel region
$\bar{t_B}$	Mean transit time through the brain
$\varepsilon(t)$	Oxygen extraction probability
V_q	Volume of blood in vessel region
x^*	Mean crowding

Appendix B

Appendix 2: Code for simulation of fixed sampling plan in chapter 5

```
MTT=100
sim_pop<-randomLHS(MTT,1)
mean_pop <- matrix(0,MTT,1)

for(i in 1:MTT){mean_pop[i] = qunif(sim_pop[i],1,15)}

fake_pop <- matrix(0,1000,MTT)

for (i in 1:MTT){
  Mean_tt = mean_pop[i]
  Scale_tt =0.5
  Rate_tt = 1/Scale_tt
  Shape_tt =Mean_tt/Scale_tt
  fake_pop[,i]=rgamma(1000, Shape_tt, Rate_tt)}
```

```
Iterations = 100 # how many times to run sampling plan

sample_sizes=c(2,5,10,15,20,25) # fixed sample sizes to test

n_plans<-length(sample_sizes)

results<-matrix(0,(n_plans*MTT*Iterations),6)

colnames(results)<-c("Sample size","Data set","Iteration","Mean est","Var est"

results[,1]<-rep(sample_sizes, each=MTT*Iterations)

results[,2]<-rep(rep(seq(1:MTT),each=Iterations),n_plans)

results[,3]<-rep(seq(1:Iterations), MTT*n_plans)

for(s in 1:length(results[,1])){
  sample_size_collected=results[,1][s]
  data_set_used=results[,2][s]
  sample_collected<-sample(fake_pop[,data_set_used],sample_size_collected)
  results[,4][s]=mean(sample_collected)
  results[,5][s]=var(sample_collected)
  results[,6][s]=(sd(sample_collected)/sqrt(sample_size_collected))/ mean(samp
}

boxplot(results[,6]~results[,1], xlab = "Sample size", ylab = "Precision ache
stop_x <- c(0, 25)
desired_D <- 0.1
```

```
stop_y <- c(desired_D, desired_D)

lines(stop_x, stop_y)

#put in function for real-mean of 6. When est_mean is greater than real_mea
threshold_value <- 6
results2 <- matrix(0, (n_plans*MTT*Iterations), 2)
colnames(results2) <- c("True mean", "Operating threshold")
for(v in 1:length(results2[,1])){
  data_set_used=results[,2][v]
  true_mean= mean(fake_pop[,data_set_used])
  results2[,1][v]=true_mean
  if(results[,4][v]<threshold_value){
    results2[,2][v]=1
  }
  else{
    results2[,2][v]=0
  }
}
big_results <- cbind(results, results2)

Ops_graph <- as.matrix(read.csv("Big_results2_Big.csv"))

OC_curve_2<-nls(Ops_graph[,2]~(1/(1+(Ops_graph[,1]/threshold_value)^b)))
y_2<-(1/(1+(Ops_graph[,1]/threshold_value)^8.413))
OC_curve_3<-nls(Ops_graph[,3]~(1/(1+(Ops_graph[,1]/threshold_value)^b)))
y_3<-(1/(1+(Ops_graph[,1]/threshold_value)^13.514))
OC_curve_4<-nls(Ops_graph[,4]~(1/(1+(Ops_graph[,1]/threshold_value)^b)))
```

```
y_4<-(1/(1+(Ops_graph[,1]/threshold_value)^17.408))
OC_curve_5<-nls(Ops_graph[,5]~(1/(1+(Ops_graph[,1]/threshold_value)^b)))
y_5<-(1/(1+(Ops_graph[,1]/threshold_value)^24.734))
OC_curve_6<-nls(Ops_graph[,6]~(1/(1+(Ops_graph[,1]/threshold_value)^b)))
y_6<-(1/(1+(Ops_graph[,1]/threshold_value)^27.19))
```

Appendix C

Appendix 3: Code for stochastic simulation in chapter 6

```
c_per_region<-c(10,50,100)

regions<-length(c_per_region)

capillaries<-sum(c_per_region)

p_ext = 0.04
p_next = 0.96
total_rate = (p_ext*c_per_region[1]+ p_ext*c_per_region[2] + p_ext*c_per_reg

iterations<- 1000

results<-matrix(0,iterations,5)
results[,1]<-seq(1,iterations,by=1)
```

```
colnames(results)<-c("Iteration","Region","Capillary","Transit time","Ext")
for(q in 1:iterations){
            propensity1<-(p_ext*c_per_region[1]/total_rate)
            propensity2<-((p_ext*c_per_region[2]/total_rate))
            propensity3<-((p_ext*c_per_region[3]/total_rate))
            t_tot<-0
        for(j in 1:5){
                dt = -log(runif(1))/total_rate
          ext = runif(1)
          t_tot<-t_tot+dt
          if(ext < propensity1){
                results[,2][q]<-1
                results[,3][q]<-sample.int(c_per_region[1],1)
                results[,4][q]<-t_tot
                results[,5][q]<-1
             break
          }
          else
          if(ext < (propensity1+propensity2))
          {
                results[,2][q]<-2
                results[,3][q]<-sample.int(c_per_region[2],1)
                results[,4][q]<-t_tot
                results[,5][q]<-1
             break
          }
          else
          if(ext < (propensity1+propensity2+propensity3)){
```

```
                results[,2][q]<-3
                results[,3][q]<-sample.int(c_per_region[3],1)
                results[,4][q]<-t_tot
                results[,5][q]<-1
            break
        }
        else
        {
                ext=0 # This reset back to proper value above.
        }
    results[,2][q]<-4
    results[,4][q]<-t_tot
    t_tot<-0
}
}
```